Furin cleaves SARS-CoV-2 spike-glycoprotein at S1/S2 and S2' for viral fusion/entry: indirect role of TMPRSS2

Rachid Essalmani[1], Jaspreet Jain[2], Delia Susan-Resiga[1,7], Ursula Andréo[1,2,7], Alexandra Evagelidis[1,7], Rabeb Mouna Derbali[1,7], David N. Huynh[1], Frédéric Dallaire[2], Mélanie Laporte[2], Adrien Delpal[3], Priscila Sutto-Ortiz[3], Bruno Coutard[4], Claudine Mapa[5], Keith Wilcoxen[5], Étienne Decroly[3], Tram NQ Pham[2], Éric A. Cohen[2,6*✉] & Nabil G. Seidah[1*✉]

[1] **Laboratory of Biochemical Neuroendocrinology Montreal Clinical Research Institute** (IRCM, affiliated to the University of Montreal) 110 Pine Ave west, Montreal, QC, H2W1R7, Canada: Rachid Essalmani, Delia Susan-Resiga, Ursula Andréo, Alexandra Evagelidis, Rabeb Mouna Derbali, David Huynh, Nabil G. Seidah

[2] **Laboratory of Human Retrovirology Montreal Clinical Research Institute** (IRCM, affiliated to the University of Montreal) 110 Pine Ave west, Montreal, QC, H2W1R7, Canada: Jaspreet Jain, Ursula Andréo, Frédéric Dallaire, Mélanie Laporte, Tram Pham, Éric A. Cohen

[3] **AFMB, CNRS**, Université Aix-Marseille, UMR 7257, Case 925, 163 Avenue de Luminy, 13288 Marseille Cedex 09, France, Marseille, France : Adrien Delpal, Priscila Sutto-Ortiz, Étienne Decroly

[4] **Unité des Virus Émergents** (UVE: Aix-Marseille Univ - IRD 190 - **Inserm** 1207 - IHU Méditerranée Infection), Marseille, France : Bruno Coutard

[5] **Boston Pharmaceuticals,** Translational Research, 55 Cambridge Parkway, Suite 400, Cambridge, MA 02142, USA: Claudine Mapa, Keith Wilcoxen

[6] These pairs of authors each contributed equally: Delia Susan-Resiga/Ursula Andreo; Alexandra Evagelidis/Rabeb Mouna Derbali.

[*]Correspondence to: seidahn@ircm.qc.ca and eric.cohen@ircm.qc.ca

Abstract

The Spike (S)-protein of SARS-CoV-2 binds host-cell receptor ACE2 and requires proteolytic "priming" (S1/S2) and "fusion-activation" (S2') for viral entry. The S-protein furin-like motifs P**R**RA**R**$_{685}$↓ and KPS**KR**$_{815}$↓ indicated that proprotein convertases promote virus entry. We demonstrate that furin and PC5A induce cleavage at both sites, ACE2 enhances S2' processing, and their pharmacological inhibition (BOS-inhibitors) block endogenous cleavages. S1/S2-mutations (μS1/S2) limit S-protein-mediated cell-to-cell fusion, similarly to BOS-inhibitors. Unexpectedly, TMPRSS2 does not cleave at S1/S2 or S2', but it can: (**i**) cleave/inactivate S-protein into S2a/S2b; (**ii**) shed ACE2; (**iii**) cleave S1-subunit into secreted S1', activities inhibited by Camostat. In lung-derived Calu-3 cells, BOS-inhibitors and μS1/S2 severely curtail "pH-independent" viral entry, and BOS-inhibitors alone/with Camostat potently reduce infectious viral titer and cytopathic effects. Overall, our results show that: furin plays a critical role in generating fusion-competent S-protein, and indirectly, TMPRSS2 promotes viral entry, supporting furin and TMPRSS2 inhibitors as potential antivirals against SARS-CoV-2.

Introduction

Epidemics date from prehistoric times but are exacerbated by overcrowding and human impact on the ecosystem[1]. The RNA coronaviruses (CoV) are zoonotic pathogens that spread in the human population, causing respiratory, enteric, renal and neurological diseases[2]. Electron microscopy of CoV revealed that the lipid envelope of each virion is surrounded by a "crown"-like structure[3], composed of multiple copies of a viral surface glycoprotein known as "spike" (S), which is essential for receptor binding and virus entry. Severe acute respiratory syndrome coronavirus (SARS-CoV-1)

and Middle East respiratory syndrome coronavirus (MERS-CoV) are two highly transmissible and pathogenic viruses that appeared in humans at the beginning of the 21st century[2, 4]. At the end of 2019, a third CoV, namely SARS-CoV-2, emerged causing widespread pandemic respiratory and vascular illnesses[5], coined COVID-19[6].

The secretory type-I membrane-bound S of SARS-CoV-2 is synthesized as a precursor glycoprotein (proS) that undergoes cleavage by host cell proteases at specific sites. During infection, the trimetric proS (monomer, 1,272 residues) is processed at an S1/S2 cleavage site by host cell proteases (Fig. 1A). This "priming" step divides the protein into two subunits S1 and S2 held together by non-covalent interactions. The N-terminal S1-ectodomain recognizes angiotensin converting enzyme-2 (ACE2) as its major entry receptor[7] *via* its receptor-binding-domain (RBD)[8] and the C-terminal membrane-anchored S2-subunit is involved in host-cell fusion and viral entry[7]. The S2-subunit contains a "fusion-activation" proteolytic site (S2'), followed by an α-helical fusion peptide (FP) and two heptad-repeat domains preceding the transmembrane domain (TM) and cytosolic tail (CT) (Fig. 1A). Cleavage of proS at S1/S2 induces a conformation change unmasking the RBD[8]. It is likely that cleavage at S2' triggers large-scale rearrangements, including a refolding step that is associated with the separation of S1- and S2-subunits and exposure of a hydrophobic α-helix C-terminal to S2', favoring fusion of viral and host cell membranes leading to virus entry[9]. Fusion with host cells can occur either at the cell surface (pH-independent) or following endocytosis of the virus (pH-dependent)[10]. However, the cognate host-cell proteases responsible for the S1/S2 and S2' cleavages are not known with certainty, as they may vary between each coronavirus and cell-type infected[7, 11-14].

The proprotein convertases (PCs; genes *PCSKs*) constitute a family of nine secretory serine proteases that regulate various processes in both health and disease states[15]. Through proteolysis, PCs are responsible for the activation and/or inactivation of many secretory precursor proteins,

including virus/pathogen surface glycoproteins[15]. Seven PCs, including the widely expressed furin, PC5A, PACE4 and PC7 cleave secretory substrates at specific single/paired basic amino acids (aa) within the motif (K/R)-X_n-(K/R)↓, where Xn= 0, 2, 4 or 6 spacer X residues[15]. Because of their critical functions, PCs, especially the ubiquitously expressed furin[16], are implicated in many viral infections *via* specific cleavages of envelope glycoproteins, a condition that allows not only the fusion of the viral lipid envelop with host cell membranes[15], but also for cell-to-cell fusion (syncytia) of certain viruses leading to important cytopathogenic effects[17, 18].

As the S1/S2 cleavage is thought to play a critical role for virus pH-independent entry, the efficacy and extent of this activation step by host proteases might be a key determinant regulating cellular tropism, viral pathogenesis and human-to-human transmission. In contrast to SARS-CoV-1, the proS of SARS-CoV-2 contains a structurally exposed P**R**RA**R**$_{685}$↓S**V** motif[7, 19] (Fig. 1A), which corresponds to a canonical furin-like cleavage site[15, 19]. This furin-like motif is presumably cleaved during *de novo* virus egress[18] for S-protein priming and may provide a key role for the efficient spread of SARS-CoV-2 to various human tissues compared to the more limited tropism of other lineage B β-coronaviruses[19, 20]. Furthermore, based on the S2' sequence of SARS-CoV-2, we proposed[19] that furin-like enzymes could also cleave the latter site at KPS**KR**$_{815}$↓S**F**[15] (Fig. 1A). In addition, it was also suggested that the cell surface type-II transmembrane serine protease 2 (TMPRSS2) independently enhances fusion by cleavage at an S2'-like site, and that S1/S2 cleavage is mostly furin-dependent[14]. However, the ability of the Arg/Lys-specific TMPRSS2 to directly cleave at S2' has not been experimentally demonstrated, but was inferred from the viral entry blockade by the relatively non-specific TMPRSS2 inhibitor Camostat[21, 22]. Thus, it is possible that one or more proteases can regulate SARS-CoV-2 entry into human airway epithelial cells[14, 20]. Furthermore, since the tissue-expression of TMPRSS2 is

restricted to a limited set of cell types compared to that of the ubiquitously expressed furin, the activity of the latter was suggested to be critical to extend viral tropism[23].

In the present study, we used various *in vitro* and *ex vivo* cell biology approaches to decipher the implication of furin-like convertases and TMPRSS2 in S-protein processing. This included the kinetic analysis of the furin-cleavage of peptides mimicking the S1/S2 and S2' sites, as well as cellular co-expression proS with the widely expressed PCs[15]. Furin and PC5A were shown to induce effective priming of proS at S1/S2 but were less efficient at cleaving S2', unless ACE2 was co-expressed. We also provide evidence that TMPRSS2 does not cleave proS at S1/S2 or S2' but it can: (**i**) cleave/inactivate proS into endoplasmic reticulum (ER)-resident S2a/S2b products; (**ii**) shed ACE2 into the medium as soluble sACE2; (**iii**) cleave the S1-subunit into a shorter secreted S1' that binds sACE2. Furthermore, we present for the first time the effectiveness of three non-toxic, cell-permeable small molecule furin-like inhibitors (BOS) that resulted in sustained intracellular inhibition of proS processing at S1/S2 and S2' by endogenous cellular furin-like proteases. All three BOS-inhibitors blocked cell-to-cell fusion and strongly impaired infection of the lung-derived epithelial cell line Calu-3 by pseudovirions or by replication-competent SARS-CoV-2, an antiviral effect potentiated by Camostat. This reveals a crucial role of furin at the portal of viral entry and highlights an indirect role of TMPRSS2 in promoting infectivity, thus supporting furin-inhibitors alone or in combination with TMRPSS2-blocking agents as potent antivirals against acute SARS-CoV-2 infection.

Results

ProS processing by furin-like convertases and TMPRSS2. The susceptibility to furin-cleavages of SARS-CoV-2' S-glycoprotein was first assessed *in vitro*. Incubation of quenched fluorogenic peptides encompassing S1/S2 and S2' sites (Supplementary Table 1), demonstrated that the S1/S2

cleavage of SARS-CoV-2 is efficiently hydrolysed by furin at pH 7.5 and less at pH 6, whereas the SARS-CoV-1 S1/S2 and MERS-CoV are poorly cleaved (Fig. 1B). Furin less efficiently cleaved the SARS-CoV-2 and MERS-CoV at S2', requiring 50-fold higher enzyme concentrations to detect cleavage (inset Fig. 1B). The high specificity of the SARS-CoV-2 to cleavage at furin-like motifs was next confirmed by demonstrating that the substitution of basic residues at the S1/S2 cleavage site (RRA**A**$_{685}$↓S, **A**RA**A**$_{685}$↓S, **A**RAR$_{685}$↓S) dramatically impaired the S1/S2 cleavage (Fig. 1C). Altogether these data showed that furin best cleaves at S1/S2 and less efficiently at S2'. Based on Camostat inhibition, TMPRSS2 was also proposed to participate in SARS-CoV-2 entry in some cells[14, 20]. Accordingly, we tested whether TMPRSS2 can cleave at S1/S2 or S2' *in vitro*. Unexpectedly, TMPRSS2 that cleaves a peptide mimicking SARS-CoV-1 at S1/S2, was unable to process SARS-CoV-2 at S1/S2 or S2' (Fig. 1D).

To further decipher the cellular role of furin-like enzymes, we expressed the S-protein in number of cell lines, whereby HeLa cells were selected as they showed evident endogenous processing of the S-protein. Thus, we co-transfected HeLa cells with a plasmid containing a codon-optimized cDNA coding for V5-tagged proS (Fig. 1A) with cDNAs encoding PC5A, furin, PC7 and PACE4[15]. Cell lysates were analyzed by Western blot (WB) after SDS-PAGE separation and probed with a V5-mAb[24]. We observed that endogenous protease(s) expressed in HeLa cells can process proS, likely at S1/S2, into a ~100 kDa S2-like product (Fig. 1E). Furthermore, only overexpression of furin and PC5A enhanced the production of the less abundant ~75 kDa S2'-like fragment (Fig. 1E). The remaining ~200 kDa proS$_{im}$ corresponds to an immature precursor form that has not exited the ER, as attested by its sensitivity to endoglycosidase-F and endoglycosidase-H (Supplementary Fig. 1A), and insensitivity to furin-like convertases that are only active in the *trans* Golgi network (TGN) and/or cell surface/endosomes[15].

The double Ala-mutant [R682A + R685A] (denoted μS1/S2) of the S1/S2 site **R**RA**R**$_{685}$↓S eliminated the P4 and P1 Arg critical for recognition by furin-like enzymes[15], and completely abrogated processing of proS at S1/S2 and putative S2' by endogenous enzymes or by overexpressed furin (Fig. 1F). These data support a role of furin in the S1/S2 cleavage and revealed that the latter may be a prerequisite for the subsequent S2' processing. The loss of furin-like cleavage at S1/S2 resulted in the accumulation of a higher molecular sized proS$_m$ (~230 kDa), which likely represents a mature form of this precursor that exited the ER and became endoglycosidase-H-resistant but remained endoglycosidase-F-sensitive (Supplementary Fig. 1A)[15, 24]. The cell-permeable PC-inhibitor decanoyl-RVKR-cmk (RVKR) effectively prevented the endogenous formation of S2, but not the cell-impermeable D6R inhibitor[24], suggesting that proS cleavage by furin into S1 and S2 occurs intracellularly and not at the cell surface (Supplementary Fig. 1B).

To better define the Arg-residues critical for processing at S1/S2, we expressed in HeLa cells the proS carrying single residue mutations: R682A, R685A and S686A in the absence or presence of overexpressed furin (Fig. 2A). The latter was based on the prediction that Ser$_{686}$ could be O-glycosylated[25], which may hamper processing at S1/S2. However, like the WT, the S686A mutant was processed by furin into S2 and S2' (Fig. 2A). The data confirmed the critical importance of P4-Arg$_{682}$ or P1-Arg$_{685}$ for the generation of S2 by endogenous furin. However, in contrast to the μS1/S2 double Ala mutant (Fig. 1F), these single mutants were partially cleaved under conditions of excess furin (Fig. 2A). This reflects the multi-basic nature of the S1/S2 recognition sequence **R**RA**R**$_{685}$↓S, whereby A**R**A**R**$_{685}$ and **RR**AA$_{685}$ are cleavable, but not ARAA$_{685}$ (μS1/S2), suggesting the importance of the P3 site[26]. Finally, Ala-mutants of each underlined residue in S2': KPS<u>KR</u>$_{815}$↓<u>S</u>FI<u>E</u>[15] resulted in an ER-retained S-protein (*not shown*).

We next examined the processing of proS by TMPRSS2 in HeLa cells (Fig. 1F). In accordance with our *in vitro* data (Fig. 1D), overexpressed TMPRSS2 did not cleave proS at S1/S2 or S2', but

rather generated two minor distinct C-terminal products, herein called S2a (~85 kDa) and S2b (~70 kDa). These fragments were seen with both wild-type (WT)-S and its μS1/S2 mutant (Fig. 1F), revealing that they are S1/S2-independent. The S2 product generated by endogenous furin-like enzymes is absent when TMPRSS2 is co-expressed with WT proS (Fig. 1F), suggesting that TMPRSS2 generates S2a and S2b before proS encounters endogenous active furin, i.e., before the TGN[27]. Indeed, like $proS_{im}$, both S2a and S2b are endoglycosidase-H-sensitive (Supplementary Fig. 1C), indicating that they are generated in the ER and can no longer exit this compartment. Thus, high levels of TMPRSS2 would effectively inactivate S2 by preventing its ER-exit to reach the cell surface. As expected, single-Arg mutations in the S1/S2 site did not affect the ability of TMPRSS2 to generate S2a and S2b (Fig. 2A).

The implication of ACE2 in the processing of proS in HeLa cells was next assessed by co-expression of proS with furin or TMPRSS2 in the absence or presence of ACE2. While not significantly affecting S1/S2 cleavage, the expression of ACE2 strongly enhanced the generation of smaller-sized S2' by furin, and S2b by TMPRSS2 (Fig. 2B), likely reflecting a change in the proS conformation upon ACE2-binding[8, 28].

Furin-inhibitors block S1/S2 cleavage, without affecting TMPRSS2 processing. We next evaluated three novel non-toxic, cell-permeable furin-inhibitors developed by Boston Pharmaceuticals available as oral (BOS-981, BOS-318) or inhalable (BOS-857) formulations (chemical motif and a representative structure of BOS-318 are shown in Figs. 3A,B). Accordingly, we first tested *in vitro* the efficacy and selectivity of these inhibitors on purified soluble forms of furin, PC5A, PACE4 and PC7. The enzymatic activity was determined using a quenched fluorogenic substrate FAM-Q**R**V**RR**AVGIDK-TAMRA, and compared to those obtained with the known PC-inhibitor RVKR-cmk[24]. The data showed that all three inhibitors

effectively blocked the processing of the above dibasic substrate by all convertases with an IC_{50} of ~7-9 nM compared to ~9-10 nM for RVKR-cmk (Fig. 3C). The furin S1/S2 cleavage was also validated *in vitro* using a 12-residue quenched fluorogenic substrate DABSYL/Glu-TNSP**RR**A**R**↓SVAS-EDANS. The inhibition deduced after hill-plot curve fitting (Fig. 3D) gave an estimated IC_{50} of 4 ± 0.7 nM (BOS-981), 32 ± 4 nM (BOS-857) and 35 ± 5 nM (BOS-318).

The inhibition of PC-activities by BOS-compounds was next assessed intracellularly using a cell-based Golgi imaging assay of U2OS cells (*see methods*). The data demonstrated that BOS-compounds inhibited endogenous furin processing of a dibasic BMP10-mimic[24] with an IC_{50} of ~8 nM *versus* 5 nM for RVKR-cmk (Fig. 3C). The above enzymatic assays showed that all 3 inhibitors can inhibit furin, but may also inhibit other members of the PC-family such as PC5A, PACE4 and PC7[15].

The effect of BOS-inhibitors was then evaluated on the processing of proS in HeLa cells stably expressing ACE2 (HeLa-ACE2; Fig. 3E). In agreement with the *in vitro* data (Fig. 3D), BOS-inhibitors blocked the S1/S2 and S2' processing by endogenous furin-like enzymes, with all three compounds showing almost complete inhibition at 300 nM (Fig. 3E), comparable to that obtained with a control 50 μM decanoyl-RVKR-cmk. In contrast, in HeLa cells none of the BOS-inhibitors affected the generation of S2a and S2b by TMPRSS2 (Supplementary Fig. 2), in agreement with the distinct cleavage specificities of furin and TMPRSS2.

TMPRSS2 sheds ACE2 and cleaves S1. Our data do not support the direct implication of TMPRSS2 in the generation of S2 or S2', since they revealed that overexpression of TMPRSS2 cleaves proS to generate ER-retained S2a and less so S2b (Fig. 1F, Supplementary Figs. 1B,C) and does not cleave proS at S2'. To verify that S2a and S2b are generated by TMPRSS2 activity in the ER, we incubated HeLa-ACE2 cells with 120 μM Camostat, known to inhibit TMPRSS2[21]. The data

showed that this inhibitor can reach the ER as it blocked the autocatalytic activation of TMPRSS2 at RQS**R**$_{255}$↓ (loss of mature ~25 kDa form in the media), prevented the formation of both S2a and S2b with increasing concentrations of TMPRSS2, and gradually allowed the resumption of the furin-like cleavage at S1/S2 (Supplementary Fig. 3A).

Accordingly, we sought to explore other functions that TMPRSS2 may exert to explain its reported enhancement of viral entry[13, 14, 20]. Hence, we expressed increasing amounts of TMPRSS2 in HeLa-ACE2 cells and followed processing and/or levels of the S1-subunit in the media by WB-analysis using an anti-S1 antibody. We showed that TMPRSS2 cleaved the furin-generated S1-subunit (~135 kDa) into a shorter S1' fragment (~115 kDa) secreted into the medium (Supplementary Fig. 3A). This cleavage may enhance the efficacy of separation of the S1-ACE2 complex and S2-domain before membrane fusion by the S2-subunit[28]. It was previously reported that TMPRSS2 sheds ACE2 into a soluble form (sACE2)[29], and the latter activity was associated with enhanced kinetics of cell-to-cell fusion (syncytia) and SARS-CoV-1 uptake. In agreement, overexpression of TMPRSS2 in HeLa-ACE2 cells enhanced the shedding of ACE2 into ~120 and ~95 kDa sACE2 forms. The generation of sACE2 and in large part S1' are both inhibited by 120 μM Camostat (Supplementary Fig. 3A). Note that the small background shedding of ACE2 is not sensitive to Camostat, suggesting that another endogenous protease, possibly ADAM17[29], is also implicated in ACE2 shedding. Co-immunoprecipitation experiments showed that sACE2 and S1' are found as a complex in the media (Supplementary Fig. 3B). Incubation of HeLa cells expressing S with media containing sACE2 and active mature ~25 kDa TMPRSS2m generated by co-expression of full length ACE2 with TMPRSS2 in HEK293 cells revealed that sACE2 enhanced the levels of S2' in cells and S1 in media (Supplementary Fig. 4A). Finally, co-expression of TMPRSS2 with WT proS or its μS1/S2 mutant in HeLa cells in the absence or presence of ACE2 resulted in the similar generation of: (**i**) secreted S1' only in the presence of ACE2 and (**ii**) secreted sACE2 (Supplementary Fig. 4B). Furthermore,

these data revealed that furin-processing at S1/S2 is not a prerequisite for these TMPRSS2-mediated cleavages.

Effect of BOS-981 on S-protein trafficking and syncytia formation. We next performed immunocytochemical analyses of HeLa cells co-expressing the WT-S-protein or its μS1/S2 mutant with ACE2 in the absence or presence of 1 μM BOS-981 under non-permeabilized (NP; S2 and ACE2 antibodies) and permeabilized (P; V5 and ACE2 antibodies) conditions (Supplementary Fig. 5). In the absence of BOS-981, the S-protein and ACE2 co-localized abundantly at the cell surface (Supplementary Fig. 5A-a). HeLa cells expressing both S-protein and ACE2 formed many syncytia, associated with reduced cell surface expression of the S-protein, and an even greater reduction of ACE2 (Supplementary Fig. 5A-b). Cells expressing both μS1/S2 and ACE2 showed an accumulation of both proS and ACE2 inside the cells and at the cell surface (Supplementary Fig. 5A-c). However, they barely induced the formation of syncytia, and when they did, the cell surface expression of S-protein and to a lesser extent ACE2 were decreased (Supplementary Fig. 5A-d). In the presence of 1 μM BOS-981, S-expressing HeLa cells (Supplementary Figs. 5B-a,b) phenocopy those expressing μS1/S2 (Supplementary Figs. 5B-c,d).

Having established that S-protein and ACE2 co-localize at the cell surface, we next analyzed the impact of furin-cleavage at S1/S2 on the ability of S-protein to induce cell-to-cell fusion. Thus, we developed a luminescence-based assay using HeLa TZM-bl reporter cells stably transfected with an HIV-1-based vector expressing luciferase under the control of the HIV-1 long terminal repeat (LTR), which can be activated by HIV Tat protein. These cells endogenously express the HIV receptor CD4 and its co-receptors CCR5 and CXCR4[30]. We postulated that fusion of donor WT HeLa cells (expressing Tat and the fusogenic S-protein) with acceptor TZM-bl cells expressing ACE2 would result in accrued luciferase activity (Fig. 4A). Indeed, as a proof-of-principle, when donor cells

expressing HIV gp160 and Tat fuse with TZM-bl acceptor cells, luciferase activity increases compared to that observed in TZM-bl control cells co-cultured with donor Hela cells expressing only Tat. (Supplementary Fig. 6C). The expression of S-protein in HeLa cells did not induce fusion with TZM-bl control cells (Supplementary Figs. 6A,C). However, ACE2 expression in TZM-bl allowed fusion with HeLa-expressing SARS-CoV-2' S-protein in a dose-dependent manner (Supplementary Fig. 6B). The linearity of our assay (correlation coefficient of 0.87) validated the use of luminescence as an indicator of cell-to-cell fusion. Conversely, expression of μS1/S2 in donor cells did not enhance fusion with TZM-bl expressing ACE2 and >60% fusion-inhibition was observed upon incubation of cells with 300 nM of BOS-inhibitors or 10 μM of the PC-inhibitor RVKR-cmk (Fig. 4B), indicating that S1/S2 cleavage promotes ACE2-dependent cell-to-cell fusion.

To assess, the role of TMPRSS2 in cell-to-cell fusion, we first co-expressed TMPRSS2 with S-protein or with μS1/S2 in donor cells. In agreement with our cell-biology data (Figs. 1F,2), TMPRSS2 abolished the fusogenic activity of S, providing evidence that TMPRSS2-mediated retention of S-protein in the ER by the generation of S2a and S2b impaired the cell-to-cell fusion activity of S-protein at the plasma membrane (Fig. 4C). However, co-expression of TMPRSS2 and ACE2 in acceptor cells tended to enhance the fusion with donor S-containing cells, an effect much more evident with μS1/S2-containing donor cells, resulting in similar cell-to-cell fusion between donor cells expressing either WT-S or μS1/S2 and acceptor ACE2-TMPRSS2 cells (Fig. 4D). This phenotype suggests that in the absence of furin-cleavage (μS1/S2) the TMPRSS2-generated S1' (Supplementary Fig. 4B) releases the N-terminal part of S1, thereby favoring furin-cleavage at S2' and cell-cell-fusion. Indeed, co-expression of ACE2 with various doses of TMPRSS2 in acceptor cells gradually promoted the fusion of the μS1/S2 to similar levels as the WT-S-induced fusion (Supplementary Fig. 7, left panels). However, sACE2 alone had no effect on μS1/S2 (Supplementary Fig. 7, right panel), as the S2' site would still be capped by the un-cleaved S1-subunit. Thus, only

high levels of TMPRSS2 in ACE2-acceptor cells allow similar fusion with donor cells expressing WT-S and μS1/S2. Interestingly, overexpression of a soluble form of ACE2 (sACE2) in acceptor cells also significantly enhanced fusion with donor cells containing WT-S (Supplementary Fig. 7, right panel). This may possibly occur *via* binding of the sACE2-S1 complex to a receptor on acceptor cells to promote cell-to-cell fusion, e.g., to integrins *via* their RGD motifs[31] or S1-binding to neuropilin1,2[32].

Effects of furin inhibitors on entry of pseudoviruses. To assess the importance of spike processing at the S1/S2 site in SARS-CoV-2 entry, we pseudotyped gp160-defective HIV with WT or μS1/S2 S-protein and tested viral entry in different target cells. Using lung Calu-3 and kidney HEK293T-ACE2 as model target cells, we found that cell-entry of viruses expressing μS1/S2 were completely defective in Calu-3, but not in 293T-ACE2 that exhibited enhanced viral-entry (Fig. 5A), similar to Vero E6 cells[33]. Since SARS-CoV-2 can enter target cells *via* "pH-independent" or "pH-dependent" pathways and the virus reportedly uses the latter to infect Vero E6 cells[34], we asked whether SARS-CoV-2 entered the 293T-ACE2 cells through the endocytic pathway. Indeed, the pH-raising chloroquine[35] efficiently blocked entry of pseudotyped SARS-CoV-2 and its μS1/S2 mutant (Supplementary Fig. 8), suggesting that in the 293T-ACE2 system, the S-protein that mediates viral entry is activated by endosomal pH-dependent proteases. This agrees with the fact that HEK293 cells allow endocytosis of pseudovirions carrying SARS-CoV-2 spike protein *via* clathrin-coated vesicles[36].

Given the contrasting effects of μS1/S2 in 293T-ACE2 and Calu-3 cells, we hypothesized that inhibiting S processing by furin-like convertases would mainly block viral entry in Calu-3 but not in 293T-ACE2 cells. Indeed, when 293T17 producing cells were treated with BOS-inhibitors during viral packaging, HIV particles expressing the WT proS-protein remained highly infectious in 293T-

ACE2 but were completely defective in Calu-3 (Fig. 5B; Supplementary Fig. 9). Thus, BOS-inhibitor treatment phenocopied the effect of the μS1/S2 in both target cells. Importantly, these phenotypes were not due to increased pseudoviral production/release since levels of HIV p24 were comparable in all cases (Fig. 5C). Similarly, in the presence of 1 μM BOS-inhibitor, processing of WT-S was clearly impaired, while the overall μS1/S2 expression profile was not affected (Fig. 5C). Collectively, our data indicate that processing of S-protein by furin-like convertases is essential for the pH-independent viral entry in Calu-3 cells but not in HEK293 cells stably expressing ACE2 where the virus enters by the endocytic pathway.

Furin-like inhibitors reduce virus production in SARS-CoV-2-infected cells. The possible antiviral effects of these furin-like inhibitors on SARS-CoV-2 replication was evaluated in Calu-3 cells pretreated with 1 μM BOS-inhibitors 24h before infection with laboratory isolated SARS-CoV-2 virus (MOI: 0.01) and harvested at 12, 24 and 48h post infection for plaque assay analysis. BOS-inhibitors significantly decreased viral titers at 12, 24 and 48h post-infection (Fig. 6A). We further evaluated the inhibitory effect of various doses of these inhibitors on the yield of infectious virus produced 24h post-infection and found that the titer of progeny viruses was reduced by more than 30-fold with 1 μM BOS-318, although the inhibitory effect could be observed starting at 0.25 μM (Fig. 6B; left panel). As well, the IC_{50} and selectivity index (SI)[37] of BOS-318 were found to be 0.2 μM and 475, respectively, underlining the inhibitor's *bona fide* efficacy (Fig. 6B; right panel). A similar analysis with BOS-857 and BOS-981 revealed comparable antiviral effects and selectivity index (Supplementary Figs. 10A,B). Importantly, the levels of viral spike (full length and cleaved S) and nucleocapsid proteins in Calu-3 cells treated with different doses of BOS-318 and the corresponding progeny virus levels were similarly decreased (Fig. 6C), underscoring the crucial role played by furin-like convertases in the

production of infectious SARS-CoV-2 during infection of lung epithelial cells. In addition, the antiviral effect of these inhibitors for SARS-CoV-2 infection was also evaluated in Vero E6, a cell target that is reported to be primarily infected *via* the endocytic pathway[7, 20]. In this system, the best inhibitory effect with 1 µM BOS-318 demonstrated a modest ~5.7-fold decrease in virus production sustained over a 12-48h infection period (Supplementary Fig. 11), possibly reflecting some furin-activity in endosomes[27].

Based on the SI of BOS-inhibitors in Vero E6 and Calu-3 cells, BOS-981 was further used in combination with Camostat to explore a potential synergistic effect of these inhibitors on viral replication in Calu-3 cells. To this end, it was observed that the two inhibitors could individually and meaningfully reduce viral replication, but their co-treatment (1 µM BOS-981 + 100 µM Camostat) inhibited >99% of progeny viruses (Fig. 6D). This highlights a synergistic effect of these drugs and the importance of endogenous furin-like proteases, and presumably TMPRSS2, in the efficient infection of Calu-3 cells by SARS-CoV-2.

Discussion

Herein, we analyzed the implication of furin[12, 14, 19, 20] and TMPRSS2[14, 20] in proS-processing, S-induced cell-to-cell fusion, SARS-CoV-2 entry and infectivity of various cell lines. *In vitro* furin cleaves at S1/S2 and S2' sites, S1/S2-cleavage activity is blocked by BOS-inhibitors (Fig. 3D), but TMPRSS2 does not cleave at either site (Figs. 1B-D). In cells furin and less so PC5A can induce an additional cleavage at S2', which is likely essential to release the fusion peptide (Fig. 1E), and S2'-processing was strongly enhanced in the presence of ACE2 (Fig. 2B). It is possible that the interaction of the S1-subunit that contains the RBD with ACE2 induces a conformational change favoring S2'-processing by cognate convertases[28]. We propose that furin first processes proS at

S1/S2, generating the cleaved S1- and S2-subunits that remain non-covalently bound[12, 38]. Separation of these subunits in the presence of ACE2 would then favor furin-cleavage at S2' and cellular fusion. BOS-inhibitors effectively blocked the generation of S2 and S2' by endogenous furin-like enzymes in HeLa-ACE2 cells (Fig. 3E). Immunocytochemical data confirmed that ACE2 co-localized at the cell surface of HeLa cells with WT-S and its μS1/S2 mutant in the presence/absence of BOS-inhibitors, suggesting that cleavage at S1/S2 does not affect the cell-surface co-localization of S-protein and ACE2 (Supplementary Fig. 5). Notably, expression of μS1/S2 or treatment with BOS-inhibitors prevented cell-to-cell fusion at the plasma membrane (Fig. 4), indicating that furin-cleavage may favor fusion at the plasma membrane and therefore allow the pH-independent entry of the virus. Thus, S-processing by furin is essential for pseudoviral entry in Calu-3 cells and abrogating this process with BOS-inhibitors effectively renders the pseudovirions defective. Finally, our data support a critical role of these furin-inhibitors to meaningfully reduce viral infection and production of infectious progeny virus in human lung cells (Fig. 6).

Unexpectedly, we showed that in HeLa and HeLa-ACE2 cells TMPRSS2 induces the cleavage of proS into S2a and S2b products in the ER (Figs. 1F, 2B). Accordingly, high levels of TMPRSS2 in donor cells expressing S-protein abolishes cell-to-cell fusion (Fig. 4C). Conversely, overexpression of cell-surface localized TMPRSS2 with ACE2 in acceptor cells slightly enhances S-induced fusion of donor cells, possibly *via* TMPRSS2 cleavage of S1 into S1' and the secretion of sACE2 that associates with S1' (Supplementary Fig. 3). The generation of S1' by TMPRSS2 likely facilitates the exposure of the S2' cleavage site[7, 33], which would then lead to more effective furin-cleavage at S2' thereby allowing membrane fusion. In agreement, donor cells synthesizing μS1/S2 only fuse with acceptor cells expressing both TMPRSS2 and ACE2 (Fig. 4D). However, our data show that virions emanating from Calu-3 cells are infectious. It is possible that the endogenous levels of TMPRSS2 in acceptor Calu-3 cells are insufficient to inactivate proS in the ER (Supplementary Fig. 3A), and that

389 at physiological levels this enzyme exerts its effects primarily at the cell surface. In addition, the
390 membrane (M)-protein and/or envelope (E)-protein of SARS-CoV-2 may shield the proS-protein
391 from early TMPRSS2-induced inactivation in the ER[39].

392 The human airway epithelium is an important site of SARS-CoV-2 infection[14, 20, 40]. The virus can
393 then disseminate to other tissues/cells such as gut, liver, endothelial cells and macrophages where
394 ACE2, furin and TMPRSS2 are co-expressed[41] and cause multi-organ dysfunction in COVID-19
395 patients[42]. The complementarity and interchangeability of these different proteases in allowing
396 SARS-CoV-2 entry into cells might explain the wider tropism of this virus compared to SARS-CoV-
397 1[43]. Our data support the presence of two different pathways of SARS-CoV-2 entry[34], and that only
398 the pH-independent pathway is efficiently inhibited by BOS ± Camostat (Figs. 5,6; model Fig. 7).
399 However, the fact that hydroxy-chloroquine therapy failed to show significant improvement in
400 COVID-19 patients[44] or in two animal models[45], suggests that the pH-independent pathway is
401 important for pathogenesis and virus propagation. This is also supported by the fact that the furin-
402 cleavage at S1/S2 has been conserved in SARS-CoV-2 isolated from human COVID-19 patients, but
403 that this site is negatively selected for after a few passages in Vero cells[46].

404 It has been proposed that injection of large amounts of recombinant human sACE2 to individuals
405 may act as an antiviral by competing with ACE2 for viral entry during the early stages of SARS-
406 CoV-2 infection[47]. Our data adds complexity to this notion, whereby only large amounts of sACE2
407 may do so. However, at physiological levels, sACE2 released by TMPRSS2 may also facilitate viral
408 entry by favoring the separation of the S1- and S2-subunits and S2' processing.

409 BOS-inhibitors represent non-toxic, small molecule inhibitors, that can be delivered orally or
410 by inhalation, and thus deserve to be rapidly tested to assess their antiviral effect against acute
411 SARS-CoV-2 infection. As observed in adult animal models, short-term inhibition of furin
412 would not cause severe side effects, despite the many physiological functions of furin[15]. The

combination of BOS- and selective TMPRSS2-inhibitors may thus offer a synergistic and effective blockade of SARS-CoV-2 entry in the lung (Figs. 6D,7) and a broad spectrum of tissues, representing a powerful antiviral strategy that deserves *in vivo* validation requiring studies in animal models.

The availability for worldwide distribution of various SARS-CoV-2 vaccines that inhibit the accessibility of the RBD of S-protein to ACE2 (https://www.raps.org/news-and-articles/news-articles/2020/3/covid-19-vaccine-tracker) represent a major therapy to block SARS-CoV-2 infections. However, it is unknown whether they will be effective in patients with impaired immune systems, and whether they will confer a persistent protection. While the protective effect of the vaccination on the whole world population remains incomplete, additional effective antiviral drugs that block viral entry in multiple organs are still needed and could help in early diagnosis of the disease. Ultimately, in case of new emerging coronavirus pandemics[48], the availability of such treatments would constitute a powerful anti-viral arsenal.

Methods

Enzymatic PC-inhibition by BOS-inhibitors

Biochemical assay: The proprotein convertases furin (108-574-Tev-Flag-6His), PC5A (PCSK5; 115-63-Tev-Flag-6His), PACE4 (PCSK6; 150-693-Tev-Flag-6His), and PC7 (PCSK7; 142-634-Tev-Flag-6His) enzymes were purified from BacMam transduced CHO cells. Reactions were performed in black 384-well polystyrene low volume plates (Greiner) at a final volume of 10 µL. BOS-inhibitors (BOS-318, BOS-857 and BOS-981) were dissolved in DMSO (1 mM) and serially diluted 1 to 3 with DMSO through eleven dilutions to provide a final compound concentration range from 0.00017 to 10 µM. 0.05 µl of each concentration was transferred to the corresponding well of an assay plate, and then 5 µl of enzyme (furin, PCSK5, PCSK6, and PCSK7) in assay buffer (100 mM HEPES pH7.5, 1 mM $CaCl_2$ and 0.005% Triton X-100) was added using a Multidrop Combi (Thermo) to the compound plates to give a final protein concentration of 0.02, 0.5, 2.5, and 1.0 nM respectively. The plates were mixed by inversion, and following a 30 min preincubation of enzyme with compound at room temperature (~22^{o}C), the substrate FAM-QRVRRAVGIDK-TAMRA (AnaSpec # 808143, 5 µl of a 1, 0.25, 0.20, and 0.5 µM solution in assay buffer for furin, PCSK5, PCSK6, and PCSK7 respectively) was added using a Multidrop Combi to the entire assay plate. The plates were centrifuged at 500Xg for 1 minute and incubated at room temperature for two hours. Enzyme inhibition was then quantified using an Envision instrument (PerkinElmer). Data were normalized to maximal inhibition determined by 1 µM Decanoyl-Arg-Val-Lys-Arg-Chloromethylketone (Calbiochem #344930).

Golgi imaging assay: This assay uses an image-based platform to evaluate the intracellular activity of furin inhibitors. Reactions were performed in black 384-well, tissue culture-treated, clear bottom plates (Greiner). Compounds under analysis were dissolved in DMSO (1.0 mM)

and serially diluted 1 to 3 with DMSO through eleven dilutions. This creates a final compound concentration range from 0.00017 to 10 µM, and 0.1 µL of each concentration was transferred to the corresponding well of the assay plate.

Cellular assay: Analyses were initiated by the addition of U2OS cells simultaneously transduced with a BacMam-delivered construct containing a Golgi-targeting sequence followed by a 12-amino acid furin/PCSK cleavage site from Bone Morphogenic Protein 10 (BMP10) and then GFP at the C terminus. The dibasic furin cleavage site sequence was flanked by glycine rich linkers (GalNAc-T2-GGGGS-DSTARIRRNAKG-GGGGS-GFP). Briefly, frozen cells are thawed in assay media (Dulbecco's Modified Eagles Medium Nutritional Mixture F-12 (Ham) without phenol red containing 5% FBS) and diluted to deliver 6000 cells/well (50 µl) to the plate using a Multidrop Combi (Thermo). After a 24-hour incubation period at 37^{o}C, the cells are stained with Cell Mask Deep Red, fixed in paraformaldehyde and the nuclei stained using Ho33342. The Golgi-targeted GFP forms bright punctate clusters within the cell. In the absence of a furin/PCSK inhibitor, the endogenous protease cleaves GFP from its N-acetylgalactosaminyltransferase-2 Golgi tether, releasing GFP into the Golgi lumen where fluorescence is diluted below the threshold of assay sensitivity. In the presence of a cell permeable furin/PCSK inhibitor, GFP fluorescence increases as intra-Golgi protease activity is reduced. Cellular GFP intensity is determined by image-based acquisition (Incell 2200, Perkin Elmer) at 40x magnification with 4 fields measured per well. Multi-scale top hat segmentation is used to identify the GFP-tagged puncta and to quantitate the average fluorescence of all puncta on a per cell basis. Cellular toxicity is determined in parallel.

Furin and TMPRSS2 fluorogenic assays: Recombinant furin was purchased from BioLegend (#719406), TRMPSS2 from Cusabio and the DABCYLGlu-EDANS labelled peptides

encompassing the different cleavage sites (Supplementary Table 1) were purchased from Genscript. Reactions were performed at room temperature in black 384-well polystyrene low volume plates (CELLSTAR-Greiner Bio-One # 784476) at a final volume of 15 µL. The fluorescent peptides were used at 5 µM and the reactions were performed in 50 mM Tris buffer (pH 6.5 or 7.5), 0.2% Triton X-100, 1mM $CaCl_2$ and furin was added at a final concentration of 2-100 nM. BOS-inhibitors (BOS-318, BOS-857 and BOS-981) were dissolved in DMSO (1 mM) and serially diluted 1 to 2 with DMSO to provide a final compound concentration range from 50 µM to 0.01 nM with 5% DMSO in the enzymatic assay. For TMPRSS2, the fluorescent peptides were used at 5 µM and the reactions were performed in 50 mM Tris buffer (pH 6.5 or 7.5), 0.2% Triton X-100, 50 mM NaCl and TMPRSS2 was added at final concentrations of 25-100 nM. Cleavage of the synthetic peptides was quantitated by determining the increase of EDANS (493 nM) fluorescence following release of the DABCYL quencher, which is excited at 335 nM using a Safire 2 Tecan fluorimeter. The fluorescence was followed during 90 min, and the enzymatic activity was deduced by measurement of the increase of fluorescence during the linear phase of the reaction. Each reaction was performed in triplicate and the standard deviation was calculated using Excel-ecart type function ($\sqrt{\frac{\sum(x-\bar{x})^2}{(n-1)}}$).

Plasmids

C-terminal V5 tagged Spike glycoprotein of SARS-CoV-2 (optimized sequence) and its mutants were cloned into the pIRES2-EGFP vector. Site-directed mutagenesis was achieved using a Quick-Change kit (Stratagene, CA) according to the manufacturer's instructions. The plasmids pCI-NEO-hACE2 received from DW Lambert (University of Leeds) and pIRES-NEO3-hTMPRSS2 from P Jolicoeur (IRCM). The ΔEnv Vpr Luciferase Reporter Vector (pNL4-3.Luc.R-E-) was obtained from Dr. Nathaniel Landau through the NIH AIDS Reagent Program

whereas the pHIV-1NL4-3 ΔEnv-NanoLuc construct was a kind gift from Dr. P Bieniasz. Plasmids encoding VSV-G, as HIV-1 Env and tat were previously described[49, 50].

Cell culture and transfection

Monolayers of HeLa, HEK293T, HEK293T17,Vero E6 and Calu-3 cells were cultured in 5% CO_2 at 37°C in Dulbecco's modified Eagle's medium (DMEM; Wisent) supplemented with 10% (v/v) fetal bovine serum (FBS; Wisent). HEK293T-ACE2[51], a generous gift from Dr. Paul Bieniasz, were maintained in DMEM containing 10% FBS, 1% nonessential amino acids (NEAA) and 50 µg/ml blasticidin (Invivogen). The cells were transfected with JetPrime transfection reagent according to the manufacturer's instructions (Polyplus transfection, New York, USA). At 24h post transfection the culture media were changed to serum-free DMEM and incubated for an additional 24h. To establish the stable HeLa cells over-expressing human ACE2, transfected cells were selected using media containing 500 µg/ml of neomycin (G418, Wisent).

To generate HIV particles pseudotyped with SARS-CoV-2 S, 293T17 cells (600,000 cells plated in a 6-well vessel) were transfected with 1 µg pNL4-3.Luc.R-E- (or pHIV-1NLΔEnv-NanoLuc) in the presence or absence of 0.3 µg pIR-2019-nCoV-S V5 plasmids using Lipofectamine-3000 (Life Technologies). In certain experiments, 293T17 cells were treated with BOS inhibitors at 6 h post transfection. Pseudovirions expressing the nano- or firefly-luciferase were collected at 24 h or 48 h post transfection, respectively. Viral supernatants were clarified by centrifugation at 300 x *g,* passed through a 0.45-µm pore-size polyvinylidene fluoride (PVDF; Millipore) syringe filter (Millipore; SLGVR33RS), and aliquots frozen at −80°C. For WB analysis of purified pseudovirions, viral supernatants were concentrated by ultracentrifugation on a 20% sucrose cushion for 3h at 35,000 RPM; Beckman Coulter OPTIMA XE; Ti70.1 rotor).

HIV particles lacking the SARS-CoV-2 S glycoprotein served as a negative control in all experiments.

Cell viability assay using MTT

Cells, seeded in a 96-well plate, the day before, at 10,000 (HEK-293T and Vero E6) or 50,000 (Calu-3) cells, were treated with serial 10-fold dilutions of BOS inhibitors for up to 48h. Cells treated with vehicle alone were used as negative control. MTT was subsequently added to the medium (final concentration: 2.5 mg/ml) and cells were further incubated for 4h at 37 ^{0}C. After removal of the culture media, DMSO was added and absorbance read at 595 nm using a microplate spectrophotometer. The data from two independent experiments done in triplicates was used to calculate the CC50 by nonlinear regression using GraphPad Prism V5.0 software.

Western blots

The cells were washed with PBS and then lysed using RIPA buffer (1% Triton X-100, 150 mM NaCl, 5 mM EDTA, and 50 mM Tris, pH 7.5) for 30 min at 4^{o}C. The cell lysates were collected after centrifugation at 14,000 × g for 10 min. The proteins were separated on 7% tris-glycine or 8% tricine gels by SDS-PAGE and transferred to a PVDF membrane (Perkin Elmer). When specified, media from cultured and transfected cells were collected and concentrated 10x using Amicon Ultra 2 ml devices with a 10 kDa cut-off (Millipore; UFC 201024), as specified by the manufacturer, and analyzed by SDS-PAGE followed by Western blotting. The proteins were revealed using a V5-monoclonal antibody (V5-mAb V2660; 1:5000; Invitrogen), ACE2 antibody (rabbit monoclonal ab108252; 1:3,000; Abcam), TMPRSS2 antibody (rabbit polyclonal; 14427-1-AP; 1:1,000; Proteintech), Actin antibody (rabbit polyclonal A2066; 1:5,000; Sigma), or SARS-CoV-2 spike antibody (rabbit polyclonal GenTex GTX135356; 1:2,000; GenTex). The antigen-antibody complexes were visualized using appropriate HRP conjugated secondary

antibodies and enhanced chemiluminescence kit (ECL; Amersham or Bio-Rad) and normalization was reported to β-actin. The quantification of the bands was performed using Image Lab software (Bio-Rad).

For analysis of SARS-CoV-2 S virions or pseudovirions, protein extracts of purified viral particles and corresponding producing cells (Calu-3 or 293T17, respectively) were resolved on 10% tris-glycine gels and immunoblotted for spike, nucleocapsid, HIV-1 Gag p24 or actin using anti-V5 (for pseudovirion detection; V2660)/anti-S2 (for virion detection; Sino Biologicals; 40590-T62), anti-N (Sino Biologicals; 40143-MM05), anti-p24 (MBS Hybridoma line 31-90-25) or anti-actin (MP Biomedicals, SKU 08691001), respectively.

Glycosidase treatment

30 to 50 µg proteins were digested for 90 min at 37^{o}C with endoglycosidase-H (Endo-H; P0702L) or endoglycosidase-F (Endo-F; P0705S) as recommended by the manufacturer (New England Biolabs).

Inhibitor treatment

At 24h post transfection, cells were incubated for 6h with two pan-PC inhibitors: the cell permeable decanoyl-RVKR-chloromethylketone (cmk; 50 mM; 4026850.001; Bachem) , or with the cell surface PC-inhibitor hexa-D-arginine (D6R; 20 µM; 344931; EMD). Culture media were then replaced with fresh ones containing the inhibitors for an additional 24h. For the selective cell-permeable furin-like inhibitors (BOS; Boston Pharmaceuticals), the cells were treated with the inhibitors at the specified concentration starting at 5h pre-transfection and throughout the duration of the experiment.

566 **Cell-to-cell fusion assay**

567 HeLa or HeLa TZM-bl cells were plated at 200,000 cells in 12-well plates. HeLa cells were
568 transiently transfected with different constructs of SARS-CoV-2 Spike or NL4.3-HIV Env, or an
569 empty vector and 0.2 µg of CMV-Tat plasmid. HeLa TZM-bl cells were transfected with human
570 ACE2, TMPRSS2 or a combination of both. At 6h post-transfection, media were replaced with
571 fresh ones containing furin-inhibitors, and 24h later the cells were detached with PBS-EDTA (1
572 µM). Different combinations of HeLa and HeLa-TZM-bl cells were placed in co-culture plate at
573 a ratio of 1:1 for a total of 60,000 cells/well of a 96 well place. After 18-24h the media were
574 removed and 50 µl of cell lysis reagent was added in each well. 20 µl of the cell lysate was used
575 for luciferase reading using 50 µl of Renilla luciferase reagent (Promega, Madison, WI, USA).
576 The relative light units (RLU) were measured using a Promega GLOMAX plate reader
577 (Promega, Madison, WI, USA) and values were reported as fold increase over the RLU
578 measured in co-culture of HeLa cells transfected EV with respective TZM-bl cells.

579 **Microscopy**

580 To establish the luciferase assay, cell co-cultures were plated on glass coverslips. After 18-24h,
581 the cells were incubated with 488 CellMask™ to stain the membrane and then fixed with 4%
582 PFA for 15 min at 4ºC. The glass coverslips were mounted on glass slides using ProLong™ Gold
583 Antifade containing DAPI (Invitrogen). The number of syncytia were counted over 10 fields.

584 **Immunofluorescence**

585 Cell culture and transfection were performed on glass coverslips. Cells were washed twice with
586 PBS and fixed with fresh 4% paraformaldehyde for 10 min at room temperature. Following
587 washes, cells were either non-permeabilized or permeabilized with 0.2% Triton X-100 in PBS
588 containing 2% BSA for 5 min, washed, and then blocking was performed with PBS containing

2% BSA for 1h. Cells were incubated with primary antibodies overnight at 4°C using an antibody against V5 (mouse monoclonal R960-25; 1:1000; Invitrogen), Spike (mouse monoclonal GTX632604; 1:500; GeneTex) and ACE2 (goat polyclonal AF933; 1:500; RnDsystems). Following wash, corresponding species-specific Alexa-Fluor (488 or 555)-tagged antibodies (Molecular Probes) were incubated for 1h at room temperature. Coverslips were mounted on a glass slide using ProLong Gold Reagent with DAPI (P36935, Life Technologies). Samples were visualized using a confocal laser-scanning microscope (LSM710, Carl Zeiss) with Plan-Apochromat 63x/1.40 Oil DIC M27 objective on ZEN software.

Pseudovirus entry

293T-ACE2 or Calu-3 (10,000 cells/well plated in a 96-well dish the day before) were incubated with up to 200 µl filtered pseudovirions for overnight. Viral inoculum was removed, then fresh media were added, and the cells cultured for up to 72h. Upon removal of spent media, 293T-ACE2 and Calu-3 cells were gently washed twice with PBS and analyzed for firefly- or nano-luciferase activity, respectively using Promega luciferase assay (Cat # E1501) or Nano-Glo luciferase system (Cat # N1110), respectively.

Replication competent SARS-CoV-2 Viruses

SARS-CoV-2, which served as the viral source, was originally isolated from a COVID-19 patient in Quebec, Canada and was designated as LSPQ1. The clinical isolate was amplified, tittered in Vero E6 using a plaque assay as detailed below, and the integrity of the S-protein multi-basic protein convertase site validated by sequencing. All experiments involving infectious SARS-CoV-2 virus were performed in the designated areas of the Biosafety level 3 laboratory (IRCM) previously approved for SARS-CoV-2 work.

612 **Plaque assay in Vero E6**

613 Vero E6 cells (1.2 x 10^5 cells/well) were seeded in quadruplicate in 24-well tissue culture plates
614 in DMEM supplemented with 10% FBS two days before infection. Cells were infected with up
615 to six ten-fold serial dilutions (10^{-2}-10^{-6}) of viral supernatant containing SARS-CoV-2 for 1h at
616 37□C (200 µl infection volume). The plates were manually rocked every 15 min during the 1-
617 hour period. Subsequently, virus was removed, cells were washed and overlaying media
618 (containing 0.6% low melt agarose in DMEM with 10% FBS) was added and incubated
619 undisturbed for 60-65h at 37□C. Post incubation, cells were fixed with 4% formaldehyde and
620 stained with 0.25% crystal violet (prepared in 30% methanol). High quality plaque pictures were
621 taken using a high resolution DLSR camera (Nikon model: D80, objective: "AF Micro-Nikkor
622 60mm f/2.8D"). Plaques were counted manually and in parallel, imaged plaque plates were
623 processed and plaques enumerated using an automated algorithm based Matlab software. Virus
624 titer is expressed as plaque-forming units per ml (PFU/ml): (number of plaques x dilution factor
625 of the virus) x 1000 / volume of virus dilution used for infection (in µl). Multiplicity of infection
626 (MOI) expressed as: MOI = PFU of virus used for infection / number of cells.

627 **Cell infections with fully replicative SARS-CoV-2**

628 Vero E.6 and Calu-3 cells were seeded in duplicates in 12-well plates (2.3 x 10^5 cells/well) the
629 day before. Cells were pre-treated with various concentrations (0.1-1µM) of BOS inhibitors and
630 vehicle alone (DMSO) for up to 24h. In certain experiments, Calu-3 were also pre-treated with
631 Camostat for 1h. Thereafter, the cells were infected with SARS-CoV-2 virus at MOI of 0.001 for
632 1h (Vero E6) or 0.01 for 3h (Calu-3 cells) in 350 µl of serum-free DMEM at 37□C with
633 occasional manual rocking of plates. Cells plus media only were used as a control. After
634 incubation, virus was removed, and the cell monolayer was washed twice successively with PBS
635 and serum-free DMEM. New media (total 1ml) containing the concentrations of BOS-inhibitors

636 was subsequently added to cells. Cell-free supernatant (250 µl) was removed at 12, 24 and 48h
637 post infection. The drugs were replenished for 1 ml media at 24h post-infection. The virus
638 supernatants were stored at -80°C until further use. Viral production in the supernatant was
639 quantified using a plaque assay on Vero E6.1 cells as described above. In certain experiments,
640 viral supernatants were harvested at the end of infection and purified on a 20% sucrose cushion
641 using ultracentrifugation as described above. The resulting concentrated virus and corresponding
642 infected cells were analyzed by Western blotting as appropriate.

643 Quantification and statistical analysis: Virus titers quantified by plaque assay in triplicate were
644 shown as mean ± standard deviation. The results from experiments done in triplicates were used
645 to calculate the IC_{50} by nonlinear regression using GraphPad Prism V5.0 software. The
646 difference between the control cells (virus with 0.001% DMSO) and the cells treated with BOS-
647 inhibitors were evaluated by Student's t test. The P values of 0.05 or lower were considered
648 statistically significant (*, $p < 0.05$; **, $p < 0.01$; ***, $p < 0.001$).

649

Acknowledgments

This work was supported in part by CIHR Foundation grants (NGS: # 148363) and (ÉAC: # 154324), a Canada Research Chairs in Precursor Proteolysis (NGS: # 950-231335), a CIHR Team Grant # HAL 157986 (NGS and ÉAC), Réseau SIDA maladies infectieuses COVID-19 initiative (ÉAC and NGS) and , ANR Reacting COVID-19 (ED and BC). The authors thank the Quebec public health laboratory for providing the infectious isolate LSPQ1 SARS-CoV-2. We thank Paul Bieniasz for the 293T-ACE2 cell line and the pHIV-1NL4-3ΔEnv-NanoLuc construct. The following reagents were obtained from the NIH AIDS Reagent Program, Division of AIDS, NIAID, NIH: TZM-bl cells, from John C. Kappes, Xiaoyun Wu, and Tranzyme, Inc. and HIV-1 pNL4-3 ΔEnv Vpr Luciferase Reporter Vector (pNL4-3.Luc.R-E-) obtained from Nathaniel Landau. We are thankful to Dominic Filion for developing the algorithm for image-assisted plaque quantification. JJ is supported by the CIHR Postdoctoral Fellowship (HIV-435243-73284). We also thank Dr Annik Prat (IRCM) for the design of the summary model shown in Fig. 7. Finally, we would like to thank Mrs. Brigitte Mary for her excellent editorial help and organization of the manuscript.

Data availability

Source data are provided with this paper. The data that support the findings of this study are preserved at repositories of the Montreal Clinical Research Institute (IRCM), Montreal, QC, Canada and available from the corresponding authors upon reasonable request.

Author contributions

RE made all the original critical experiments of the implication of the PCs in Spike processing and the effect of their inhibitors. JJ performed all the cell assays with infectious SARS-CoV-2. DSR participated in the biochemical characterizations of TMPRSS2 processing of ACE2 and S1. UA performed all cell-cell fusion assays. AE made all the mutants used in the work. RMD generated the HeLa-ACE2 cells and prepared all the cells for *ex vivo* analyses. DNH performed all the immunocytochemical experiments. DF performed the proteomics mass spectral analysis of S2 and S2'. FD and ML performed the experiments related to SARS-CoV-2 pseudovirions. AD and PSO performed all the furin and TMPRSS2 *in vitro* kinetic cleavage analyses of peptides mimicking the S1/S2 and S2' sites. CM and KW provided the BOS-inhibitors and their characterization. ED made seminal contributions to the possible role of furin-like enzymes in the processing of the spike glycoprotein and actively contributed to the conceptualization and writing of the manuscript. TNQP designed most of the viral experiments and data analyses. EAC (virology) and NGS (biochemistry and cell biology) conceptualized the research program and provided the intellectual contributions and funding for the whole project. All authors actively contributed to the final version of the manuscript.

References

1. Dobson AP, Carper ER. Infectious Diseases and Human Population History: Throughout history the establishment of disease has been a side effect of the growth of civilization. *Bioscience* **46**, 115-126 (1996).
2. Cui J, Li F, Shi ZL. Origin and evolution of pathogenic coronaviruses. *Nat Rev Microbiol* **17**, 181-192 (2019).
3. Almeida JD, Tyrrell DA. The morphology of three previously uncharacterized human respiratory viruses that grow in organ culture. *J Gen Virol* **1**, 175-178 (1967).
4. Belouzard S, Millet JK, Licitra BN, Whittaker GR. Mechanisms of coronavirus cell entry mediated by the viral spike protein. *Viruses* **4**, 1011-1033 (2012).
5. Liu PP, Blet A, Smyth D, Li H. The Science Underlying COVID-19: Implications for the Cardiovascular System. *Circulation* **142**, 68-78 (2020).
6. The species Severe acute respiratory syndrome-related coronavirus: classifying 2019-nCoV and naming it SARS-CoV-2. *Nat Microbiol* **5**, 536-544 (2020).
7. Tang T, Bidon M, Jaimes JA, Whittaker GR, Daniel S. Coronavirus membrane fusion mechanism offers as a potential target for antiviral development. *Antiviral Res*, 104792 (2020).
8. Lan J, *et al.* Structure of the SARS-CoV-2 spike receptor-binding domain bound to the ACE2 receptor. *Nature* **581**, 215-220 (2020).
9. Lu G, Wang Q, Gao GF. Bat-to-human: spike features determining 'host jump' of coronaviruses SARS-CoV, MERS-CoV, and beyond. *Trends Microbiol* **23**, 468-478 (2015).
10. Millet JK, Whittaker GR. Physiological and molecular triggers for SARS-CoV membrane fusion and entry into host cells. *Virology* **517**, 3-8 (2018).
11. Ou X, *et al.* Characterization of spike glycoprotein of SARS-CoV-2 on virus entry and its immune cross-reactivity with SARS-CoV. *Nat Commun* **11**, 1620 (2020).
12. Hoffmann M, Kleine-Weber H, Pöhlmann S. A Multibasic Cleavage Site in the Spike Protein of SARS-CoV-2 Is Essential for Infection of Human Lung Cells. *Mol Cell* **78**, 779-784.e775 (2020).
13. Shang J, *et al.* Cell entry mechanisms of SARS-CoV-2. *Proc Natl Acad Sci U S A* **117**, 11727-11734 (2020).
14. Bestle D, *et al.* TMPRSS2 and furin are both essential for proteolytic activation of SARS-CoV-2 in human airway cells. *Life Sci Alliance* **3**, (2020).
15. Seidah NG, Prat A. The biology and therapeutic targeting of the proprotein convertases. *Nat Rev Drug Discov* **11**, 367-383 (2012).
16. Van de Ven WJ, Creemers JW, Roebroek AJ. Furin: the prototype mammalian subtilisin-like proprotein-processing enzyme. Endoproteolytic cleavage at paired basic residues of proproteins of the eukaryotic secretory pathway. *Enzyme* **45**, 257-270 (1991).
17. Moulard M, Decroly E. Maturation of HIV envelope glycoprotein precursors by cellular endoproteases. *Biochim Biophys Acta* **1469**, 121-132 (2000).
18. Millet JK, Whittaker GR. Host cell proteases: Critical determinants of coronavirus tropism and pathogenesis. *Virus Res* **202**, 120-134 (2015).

19. Coutard B, Valle C, de Lamballerie X, Canard B, Seidah NG, Decroly E. The spike glycoprotein of the new coronavirus 2019-nCoV contains a furin-like cleavage site absent in CoV of the same clade. *Antiviral Res* **176**, 104742 (2020).
20. Hoffmann M, *et al.* SARS-CoV-2 Cell Entry Depends on ACE2 and TMPRSS2 and Is Blocked by a Clinically Proven Protease Inhibitor. *Cell* **181**, 271-280.e278 (2020).
21. Kawase M, Shirato K, van der Hoek L, Taguchi F, Matsuyama S. Simultaneous treatment of human bronchial epithelial cells with serine and cysteine protease inhibitors prevents severe acute respiratory syndrome coronavirus entry. *J Virol* **86**, 6537-6545 (2012).
22. Nimishakavi S, Raymond WW, Gruenert DC, Caughey GH. Divergent Inhibitor Susceptibility among Airway Lumen-Accessible Tryptic Proteases. *PLoS One* **10**, e0141169 (2015).
23. Cyranoski D. Profile of a killer: the complex biology powering the coronavirus pandemic. *Nature* **581**, 22-26 (2020).
24. Susan-Resiga D, *et al.* Furin Is the Major Processing Enzyme of the Cardiac-specific Growth Factor Bone Morphogenetic Protein 10. *J Biol Chem* **286**, 22785-22794 (2011).
25. Andersen KG, Rambaut A, Lipkin WI, Holmes EC, Garry RF. The proximal origin of SARS-CoV-2. *Nat Med* **26**, 450-452 (2020).
26. Örd M, Faustova I, Loog M. Biochemical evidence of furin specificity and potential for phospho-regulation at Spike protein S1/S2 cleavage site in SARS-CoV2 but not in SARS-CoV1 or MERS-CoV. *bioRxiv*, 2020.2006.2023.166900 (2020).
27. Thomas G. Furin at the cutting edge: from protein traffic to embryogenesis and disease. *Nature Reviews Molecular Cell Biology* **3**, 753-766 (2002).
28. Benton DJ, *et al.* Receptor binding and priming of the spike protein of SARS-CoV-2 for membrane fusion. *Nature* **588**, 327-330 (2020).
29. Heurich A, Hofmann-Winkler H, Gierer S, Liepold T, Jahn O, Pöhlmann S. TMPRSS2 and ADAM17 cleave ACE2 differentially and only proteolysis by TMPRSS2 augments entry driven by the severe acute respiratory syndrome coronavirus spike protein. *J Virol* **88**, 1293-1307 (2014).
30. Platt EJ, Wehrly K, Kuhmann SE, Chesebro B, Kabat D. Effects of CCR5 and CD4 cell surface concentrations on infections by macrophagetropic isolates of human immunodeficiency virus type 1. *J Virol* **72**, 2855-2864 (1998).
31. Sigrist CJ, Bridge A, Le Mercier P. A potential role for integrins in host cell entry by SARS-CoV-2. *Antiviral Res* **177**, 104759 (2020).
32. Daly JL, *et al.* Neuropilin-1 is a host factor for SARS-CoV-2 infection. *Science* **370**, 861-865 (2020).
33. Walls AC, Park YJ, Tortorici MA, Wall A, McGuire AT, Veesler D. Structure, Function, and Antigenicity of the SARS-CoV-2 Spike Glycoprotein. *Cell* **181**, 281-292.e286 (2020).
34. Hoffmann M, *et al.* Chloroquine does not inhibit infection of human lung cells with SARS-CoV-2. *Nature* **585**, 588-590 (2020).
35. Vincent MJ, *et al.* Chloroquine is a potent inhibitor of SARS coronavirus infection and spread. *Virol J* **2**, 69 (2005).
36. Bayati A, Kumar R, Francis V, McPherson P. SARS-CoV-2 infects cells following viral entry via clathrin-mediated endocytosis.). bioRxiv (2020).
37. Cheng YW, *et al.* Furin Inhibitors Block SARS-CoV-2 Spike Protein Cleavage to Suppress Virus Production and Cytopathic Effects. *Cell Rep* **33**, 108254 (2020).

38. Cai Y, *et al.* Distinct conformational states of SARS-CoV-2 spike protein. *Science* **369**, 1586-1592 (2020).
39. Malik YA. Properties of Coronavirus and SARS-CoV-2. *Malays J Pathol* **42**, 3-11 (2020).
40. Wölfel R, *et al.* Virological assessment of hospitalized patients with COVID-2019. *Nature* **581**, 465-469 (2020).
41. Zhou L, *et al.* The SARS-CoV-2 targets by the pscRNA profiling of ACE2, TMPRSS2 and Furin proteases. *iScience*, 101744 (2020).
42. Mokhtari T, Hassani F, Ghaffari N, Ebrahimi B, Yarahmadi A, Hassanzadeh G. COVID-19 and multiorgan failure: A narrative review on potential mechanisms. *J Mol Histol* **51**, 613-628 (2020).
43. Chu H, *et al.* Comparative tropism, replication kinetics, and cell damage profiling of SARS-CoV-2 and SARS-CoV with implications for clinical manifestations, transmissibility, and laboratory studies of COVID-19: an observational study. *Lancet Microbe* **1**, e14-e23 (2020).
44. Self WH, *et al.* Effect of Hydroxychloroquine on Clinical Status at 14 Days in Hospitalized Patients With COVID-19: A Randomized Clinical Trial. *JAMA* **324**, 2165-2176 (2020).
45. Rosenke K, *et al.* Hydroxychloroquine prophylaxis and treatment is ineffective in macaque and hamster SARS-CoV-2 disease models. *JCI Insight* **5**, (2020).
46. Peacock TP, *et al.* The furin cleavage site of SARS-CoV-2 spike protein is a key determinant for transmission due to enhanced replication in airway cells. *bioRxiv*, 2020.2009.2030.318311 (2020).
47. Monteil V, *et al.* Human soluble ACE2 improves the effect of remdesivir in SARS-CoV-2 infection. *EMBO Mol Med*, e13426 (2020).
48. Morens DM, Fauci AS. Emerging Pandemic Diseases: How We Got to COVID-19. *Cell* **183**, 837 (2020).
49. Lodge R, Lalonde JP, Lemay G, Cohen EA. The membrane-proximal intracytoplasmic tyrosine residue of HIV-1 envelope glycoprotein is critical for basolateral targeting of viral budding in MDCK cells. *EMBO J* **16**, 695-705 (1997).
50. Forget J, Yao XJ, Mercier J, Cohen EA. Human immunodeficiency virus type 1 vpr protein transactivation function: mechanism and identification of domains involved. *J Mol Biol* **284**, 915-923 (1998).
51. Schmidt F, *et al.* Measuring SARS-CoV-2 neutralizing antibody activity using pseudotyped and chimeric viruses. *J Exp Med* **217**, (2020).

Figure legends

Figure 1: **Processing of S-peptides and S-protein. (A)** Schematic representation of the primary structure of preproS and its domains and the predicted furin-like S1/S2 site generating the S1- and S2-subunits, as well as the S2' site preceding the fusion peptide (FP). The signal peptide (SP), N-terminal domain (NTD), receptor binding domain (RBD) to ACE2, the two heptad repeats HR1 and HR2, the transmembrane domain (TM), the cytosolic tail (CT) and the C-terminal V5-tag are indicated. **(B-D)** *In vitro* furin and TMPRSS2 cleavage activity against the synthetic peptides described in Table 1. Each substrate was tested at a final protease concentration of 2 and 100 nM (furin, enlarged box) and 50 nM (TMPRSS2) at pH 6 and 7.5 respectively. **(B)** *In vitro* furin activity against the peptides mimicking the S1/S2 and S2' cleavage site sequence of the spike protein from SARS-CoV-1, SARS-CoV-2 and MERS-CoV. **(C)** *In vitro* furin activity against WT and mutated peptides carrying substitutions in the furin-like cleavage site mimicking the S1/S2 SARS-CoV-2 cleavage site. **(D)** TMPRSS2 does not cleave at either S1/S2 or S2'. (**E**) Western blot analyses of the processing of WT proS into V5-tagged S2 and S2' by the proprotein convertases furin, PC5A, PACE4 and PC7 following co-transfection of their cDNAs in HeLa cells. The migration positions of immature $proS_{im}$, S2 and S2', as well as the actin loading control are emphasized. V = empty pIRES-EGFP-V5 vector. **(F)** Western blot analyses of HeLa cells following co-transfection with cDNAs coding for either WT S-protein or its double Ala-mutant [R685A + R682A] (μS1/S2) in the absence or presence of cDNAs coding for furin or TMPRSS2 at an S:protease ratio of 1:2. *Inconsistently observed oligomeric forms of proS. **(E, F)** The estimated % cleavages into S1/S2 and S2' are shown, based on the ratio of the V5-immunoreactivity of the cleaved form to the sum of all forms. The data are representative of at least three independent experiments.

Figure 2: **Comparative processing of proS and its S1/S2 mutants by endogenous proteases in HeLa cells and upon co-expression of furin or TMPRSS2.** (**A**) Hela cells were transiently co-transfected with cDNAs coding for an empty vector (V), vectors encoding furin, TMPRSS2 and WT spike glycoprotein or its PC-cleavage sites mutants at positions P4 (R682A), P1 (R685A) and P1' (S686A). At 24h post-transfection cell lysates were subjected to Western blotting using a V5-mAb. *Inconsistently observed oligomeric forms of proS. (**B**) Western blot showing the impact of ACE2 on the processing of spike glycoprotein by furin and TMPRSS2. The ratio of cDNAs used was S:ACE2:TMPRSS2 = 1:1:2. The percent processing shown under each lane was calculated from the ratio of the V5-imunoreactivity of each protein relative to the total V5-immunoreactivity. The data are representative of at least three independent experiments.

Figure 3: **Inhibition of PCs by BOS compounds.** (**A**) Chemical motif of BOS-inhibitors. (**B**) Representative structure of BOS-318. (**C**) *In vitro* BOS-inhibition of the cleavage of the fluorogenic dibasic substrate FAM-QRVRRAVGIDK-TAMRA by each of the proprotein convertases furin, PC5A (PCSK5), PACE4 (PCSK6) and PC7 (PCSK7). All experiments were performed in 10 different wells and the average pIC_{50} (in nM) was calculated. For comparison we present the inhibitory pIC_{50} of the furin-like inhibitor RVKR-cmk performed >100 times. Golgi assay: Last column represents the effects of BOS-inhibitors on U2OS cells expressing each of furin, PC5A, PACE4 and PC7 simultaneously transduced with a BacMam-delivered construct containing a Golgi-targeting sequence followed by a 12-amino acid furin/PCSK cleavage site from Bone Morphogenic Protein 10 (BMP10) and then GFP at the C terminus (GalNAc-T2-GGGGS-DSTARIRR↓NAKG-GGGGS-GFP). Dibasic cleavage releases NAKG-GGGGS-GFP thereby reducing the Golgi-associated fluorescence estimated by imaging. (**D**) *In vitro* inhibition of Furin by the BOS compounds. Furin (2 nM) was incubated with increasing concentration of BOS-inhibitors, and its enzymatic activity against the synthetic peptides

DABSYL/Glu-TNSP**RR**A**R**↓SVAS-EDANS (5 µM) was determined at pH 7.5 (n=3). (**E**) Furin-inhibitors (BOS) abrogate endogenous processing of the spike glycoprotein. Hela cells were transiently transfected with a cDNA encoding an empty vector (V) or with one expressing the V5-tagged spike (S) glycoprotein (Spike-V5). At 5h pre-transfection, cells were treated with vehicle DMSO (NT, duplicate) or with the furin-inhibitors at indicated concentrations, or RVKR-cmk at 50 µM. At 24h post-transfection media were replaced with fresh ones lacking (NT) or containing the inhibitors for an additional 24h. Cell extracts were analyzed by Western blotting using a mAb-V5. All data are representative of at least three independent experiments.

Figure 4: **Spike-induced cell-to-cell fusion relies on furin cleavage at S1/S2.** (**A**) Cell-to-cell fusion between donor cells (HeLa) expressing the fusogenic SARS-CoV-2 Spike protein along with the HIV trans-activator Tat, and acceptor cells (TZM-bl) that express ACE2. Upon fusion, Tat is transferred from donor to acceptor cells, thereby inducing luciferase expression. (**B**) Donor cells were transfected with vectors expressing either no protein (empty vector, EV), µS1/S2 , or WT Spike (S) in the absence (S) or presence of vehicle (S-DMSO) and the furin-inhibitors RVKR (10 µM), BOS-318, BOS-981, BOS-857 (300 nM). Acceptor cells were transfected with a vector expressing ACE2. After 48h, donor and acceptor cells were co-cultured for 18h. Relative luminescence units (RLU) were normalized to the EV value arbitrarily set to 1. Data are presented as mean values ± SD (n=3), One-Way ANOVA, Dunn-Sidàk multiple comparison test. (**C**) Donor HeLa cells were co-transfected with vectors (1:1 ratio) expressing WT Spike, µS1/S2 with EV or TMPRSS2. Acceptor TZM-bl cells were transfected with ACE2. After 48h, HeLa and TZM-bl were co-cultured for 18h and luciferase activity measured. The fusion is represented as ratio between the RLU measured for each condition and the RLU measured in the co-culture between donor cells transfected with EV and ACE2 acceptor cells.

Data are presented as mean values ± SD (n=3), One-Way ANOVA, Bonferroni multiple comparison test. (**D**) Donor HeLa cells expressing WT S or μS1/S2 were co-cultured with acceptor TZM-bl cells expressing (ratio of 1:1): EV + EV, ACE2 + EV, ACE2 + TMPRSS2 or TMPRSS2 + EV. The extent of fusion is represented as a ratio between the RLU measured for each condition and that of donor cells expressing EV. The bar graph represents the average of 3 experiments performed in triplicates. Data are presented as mean values ± SEM (n=3), Two-Way ANOVA.

Figure 5: **Processing of SARS-CoV-2 S by furin-like convertases is essential for viral entry in human lung epithelial cells but not in model HEK 293 cells stably expressing ACE2**. (**A**) Furin cleavage of proS at the S1/S2 site is required for SARS-CoV-2 pseudoviral entry in Calu-3 but not 293T-ACE2. Cells were inoculated with luciferase-expressing HIV particles pseudotyped with SARS-CoV-2 wild-type Spike (WT S) or mutated S (μS1/S2). Each dot represents a different experiment with median luciferase activity calculated from three biological replicates. Three or four experiments were performed for each cell type. Error bars indicate standard deviation (SD) (**B**) Inhibiting proS processing at S1/S2 by a novel furin-like inhibitor (BOS-318) during pseudovirion packaging prevents viral entry in Calu-3 but not in 293T-ACE2 Each dot color depicts a different experiment and shown is mean ± SD of two to three experiments (three biological replicates per experiment). (**C**) Western blot analysis show BOS-318 inhibits processing of proS at the S1/S2 site. Purified pseudovirions and cellular extracts of producing 293T17 cells treated or not with BOS-318 inhibitor were separated on SDS-PAGE gel and analyzed for HIV-1 p24 and V5-tagged S-protein (proSm or cleaved, S2) as indicated.

Figure 6: **Furin-like inhibitors and Camostat Treatment decrease SARS-CoV-2 infection in Calu-3 Cells. (A)** Replication kinetics was studied at 12, 24 and 48h post-infection by plaque

assay to determine PFUs of SARS-CoV-2 virus in the supernatant of infected Calu-3 cells treated or not with 1μM BOS-318, BOS-857 and BOS-981. A line graph represents results of the triplicate plaque assay results (mean ± SD). **(B)** The virus titers (PFU per milliliter) released in the supernatant (24h post-infection) of infected Calu-3 cells treated with indicated concentrations of BOS-318 were determined by plaque assay (mean ± SD of triplicates, *, $p < 0.05$; **, $p < 0.01$; ***, $p < 0.001$) (left panel). The selectivity index (SI) of BOS-318 in Calu-3 cells as shown in top right panel was determined by CC_{50}/IC_{50}. The left y axis indicates the inhibition of virus titer (percent) relative to that of the untreated control group (red). The right y axis indicates the cell viability (percent) relative to that of the untreated control group (green). The CC_{50} (50% cytotoxic concentration), IC_{50} (half maximal inhibitory concentration), and SI (selectivity index) values for each inhibitor are as shown. Representative plaque images of infected Calu-3 cells treated with indicated doses of BOS-inhibitors are shown in the bottom right panel. **(C)** Immunoblots for the infected Calu-3 cells (right panel) and viral particles secreted in the supernatant (left panel) with and without treatment with BOS-inhibitors indicate reduced viral protein levels. Immunoblots were probed for the full-length (proSm) and cleaved (S2) fragments of viral S protein and nucleocapsid (N) protein as indicated; β-Actin was included as the loading control for the cells. **(D)** The virus titers (PFU per milliliter) released in the supernatant (24h post-infection) of infected Calu-3 cells treated with BOS-981 and/or Camostat (Camo) were determined by plaque assay (mean ± SD of duplicates, *, $p < 0.05$; **, $p < 0.01$; ***, $p < 0.001$) (top panel). Representative plaque images of infected Calu-3 cells are shown in the bottom panel.

Figure 7: **Proposed model for the processing of S-protein and its blockade by furin and TMPRSS2 inhibitors.** Boxed left panel: schematic representation of the S-glycoprotein domains of SARS-CoV-2, including the N-terminal (NTD) and C-terminal (CTD) domains of S1, the

furin-S1/S2 and S2' and the TMPRSS2 S1' processing sites and the fusogenic α-helix that follows S2'. Binding of the RBD domain of S1 to the membrane associated ACE2 in target cells, and the cell surface expression of TMPRSS2 and furin are also schematized. Right panels: (**1**) Viral infection is favored by the presence of a furin-like sites at S1/S2 and S2'. TMPRSS2 in acceptor cells enhances infection by shedding ACE2 into soluble sACE2 (in bold) and is further enhanced by cleavage of S1 into S1' which forms a secreted complex with sACE2. Optimal blockade of viral infection is achieved by a combination of furin and TMPRSS2 inhibitors. (**2**) In absence of a furin-like site at S1/S2 (μS1/S2), high levels of TMPRSS2 in acceptor cells can favor infection by cleaving S1 into S1' and shedding ACE2 into soluble sACE2 complexed with S1'.

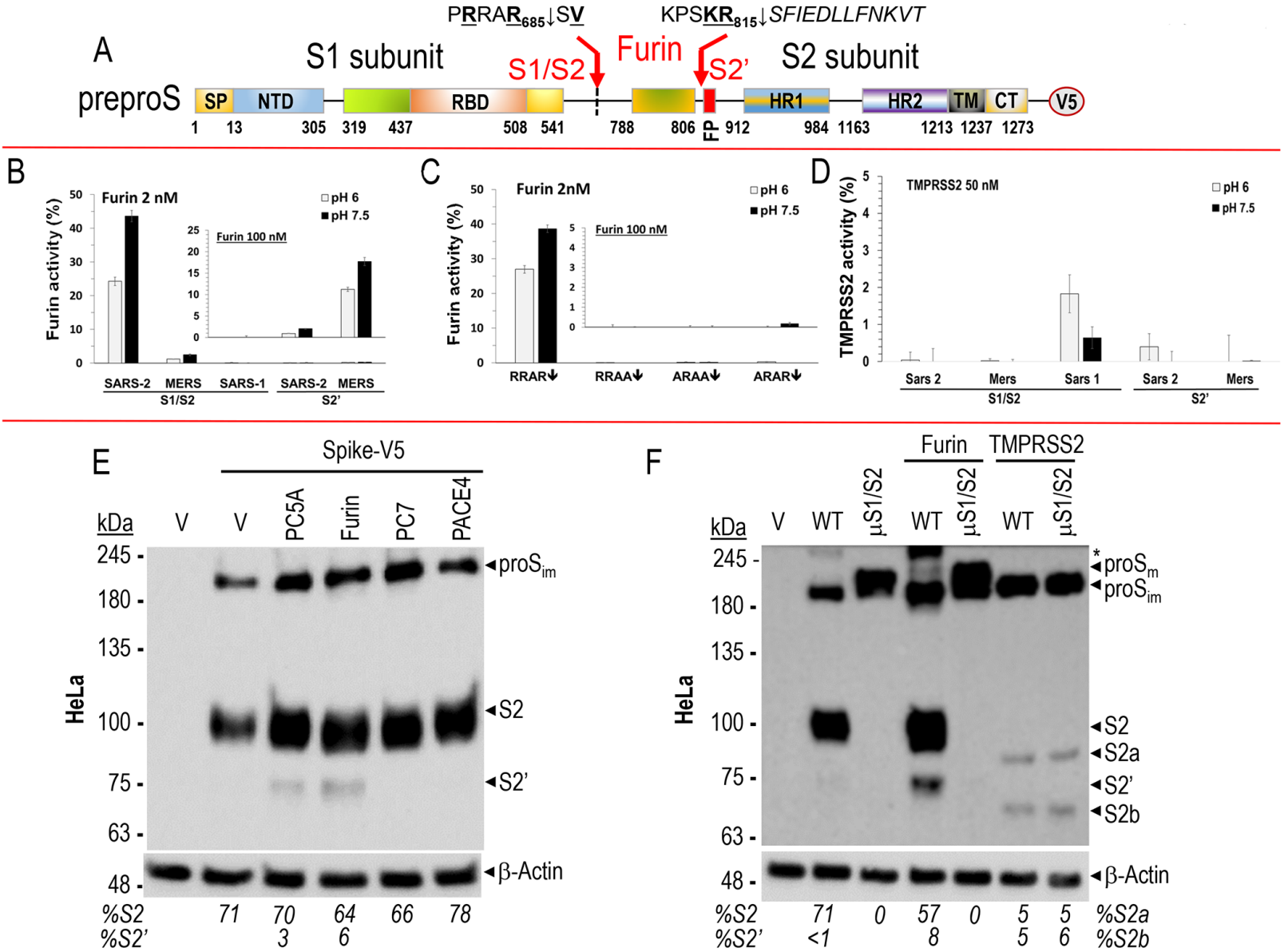

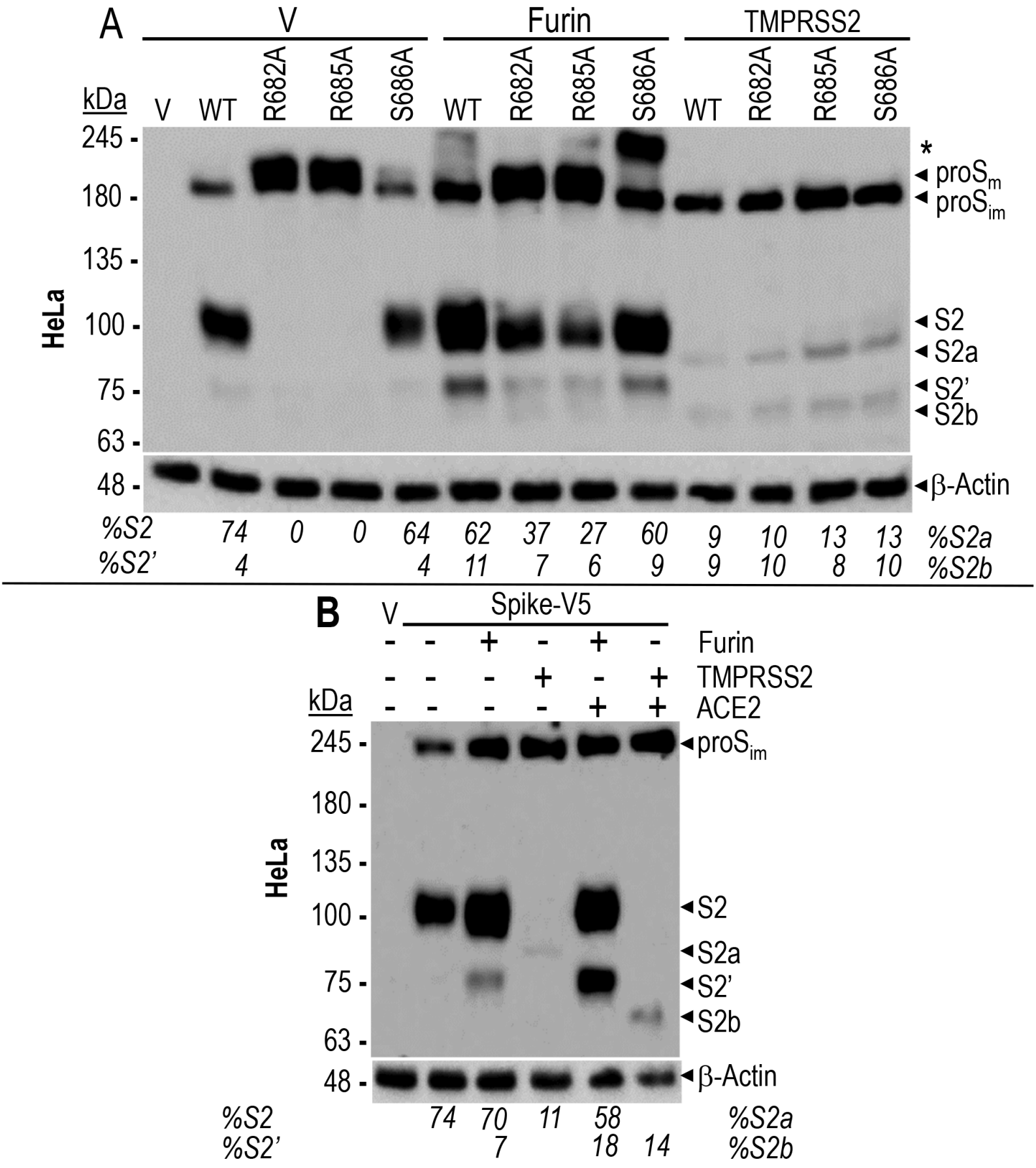

A

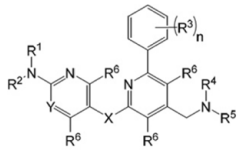

Structure of Furin inhibitors

B

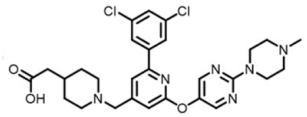

BOS-318

C

	Furin pIC50	PCSK5 pIC50	PCSK6 pIC50	PCSK7 pIC50	Golgi pIC50 (U2OS)
BOS-318	8.8 ± 0.4 (n = 10)	7.6 ± 0.09 (n = 8)	6.7 ± 0.15 (n = 6)	7.4 ± 0.22 (n = 8)	7.7 ± 0.24 (n = 22)
BOS-981	9.3 ± 0.5 (n = 10)	7.5 ± 0.22 (n = 10)	6.9 ± 0.1 (n = 4)	6.9 ± 0.2 (n = 8)	8.3 ± 0.25 (n = 12)
BOS-857	9.4 ± 0.3 (n = 10)	7.6 ± 0.1 (n = 10)	6.7 ± 0.24 (n = 5)	6.9 ± 0.3 (n = 8)	7.6 ± 0.2 (n = 12)
Decanoyl-RVKR-CMK "Furin Inhibitor I"	9.1 ± 0.43 (n = 447)	9.9 ± 0.38 (n = 162)	9.2 ± 0.24 (n = 214)	9.6 ± 0.63 (n = 198)	5.1 ± 0.33 (n = 8)

D

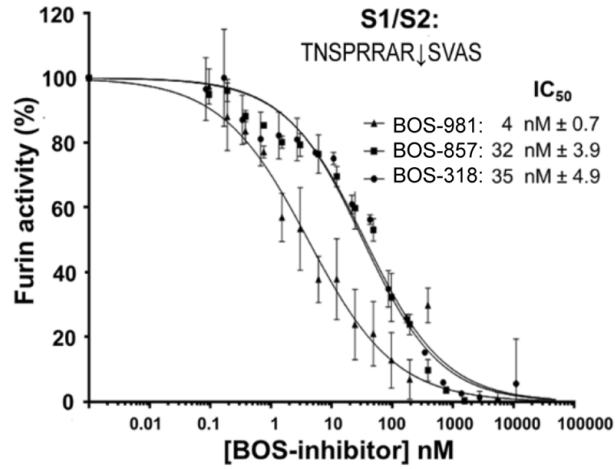

E

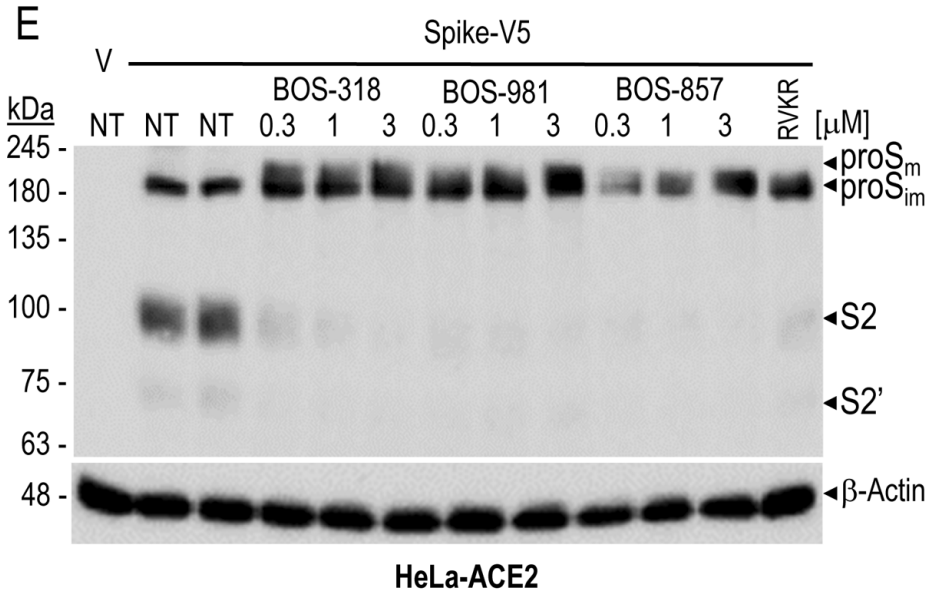

HeLa-ACE2

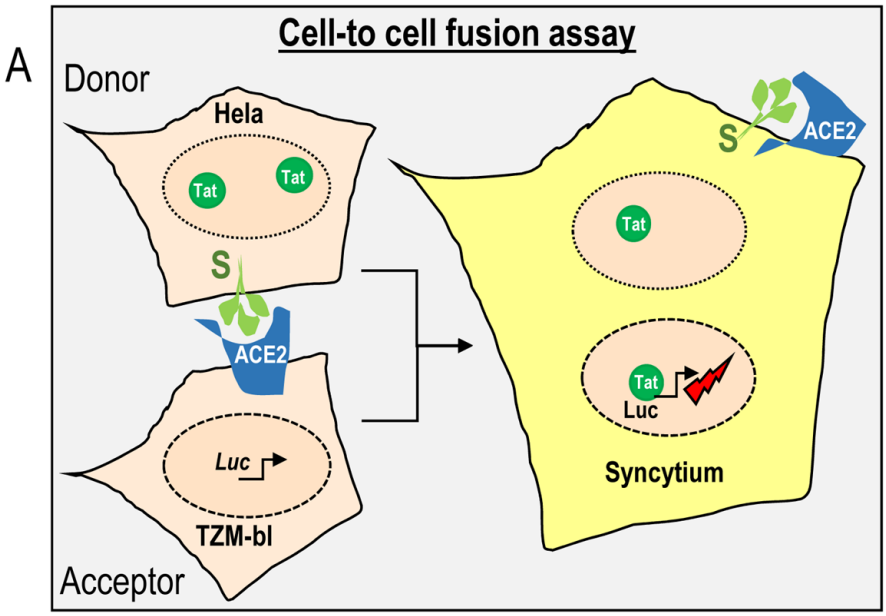

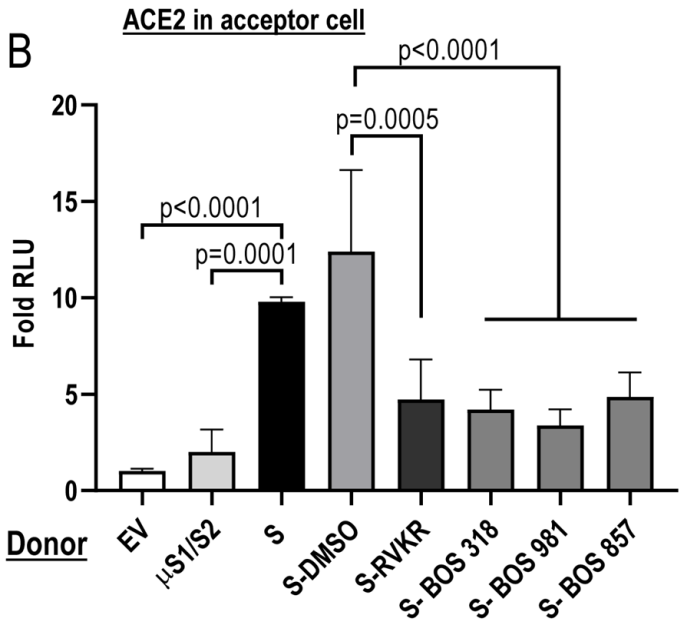

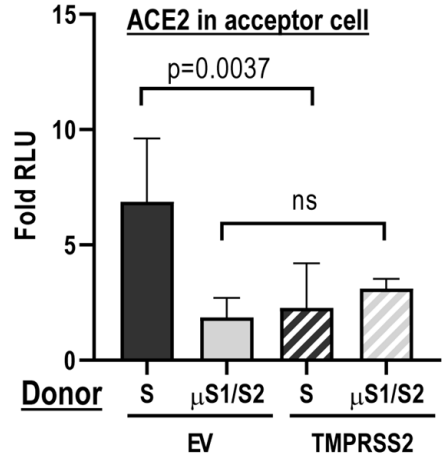

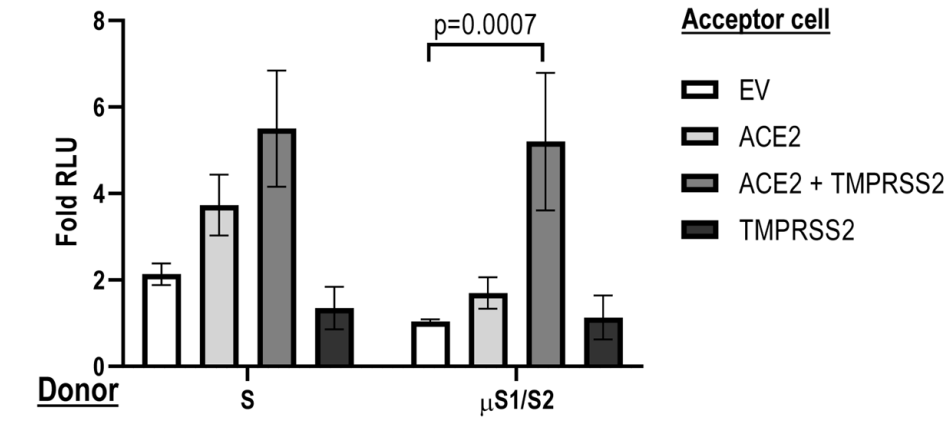

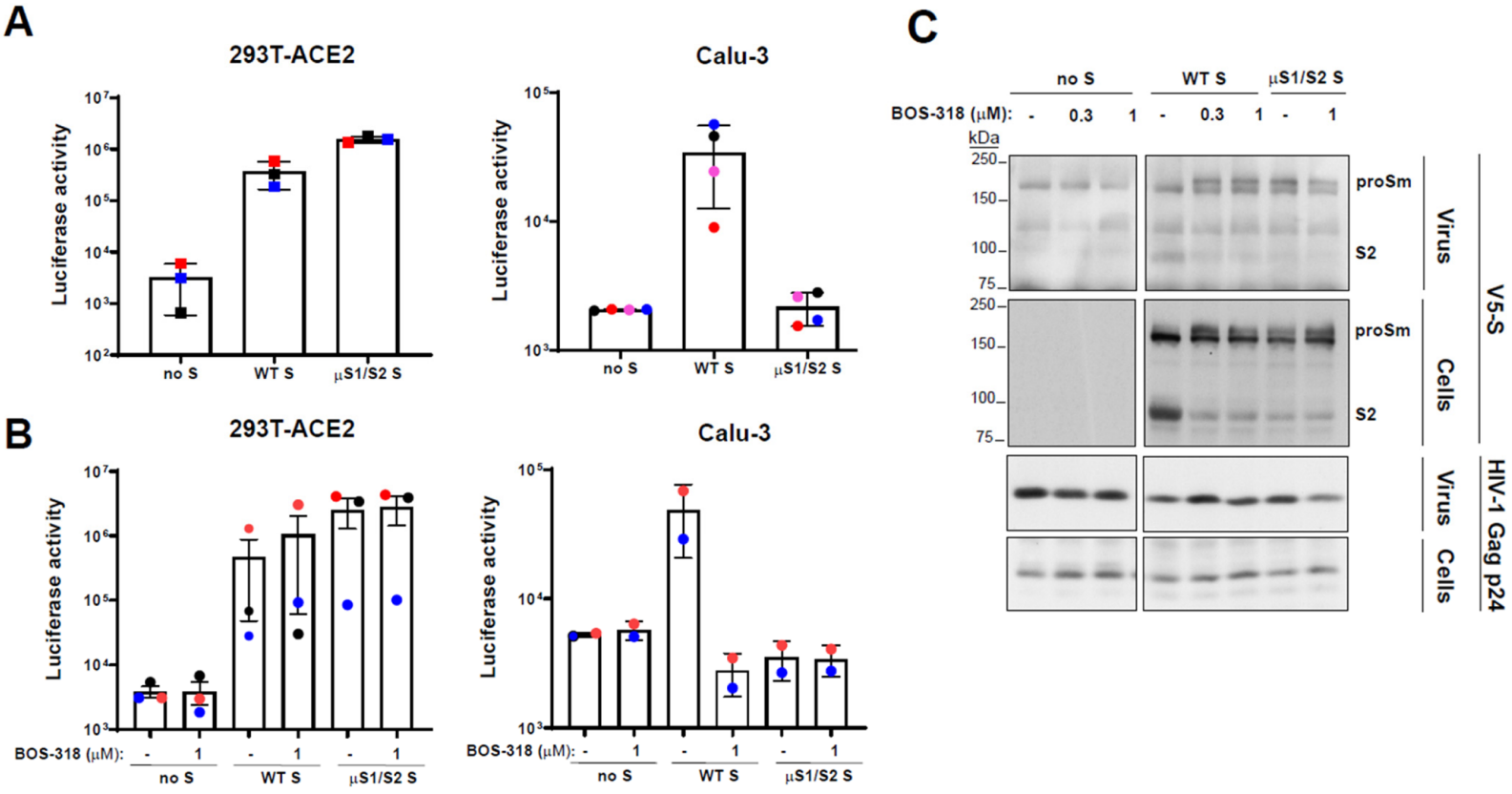

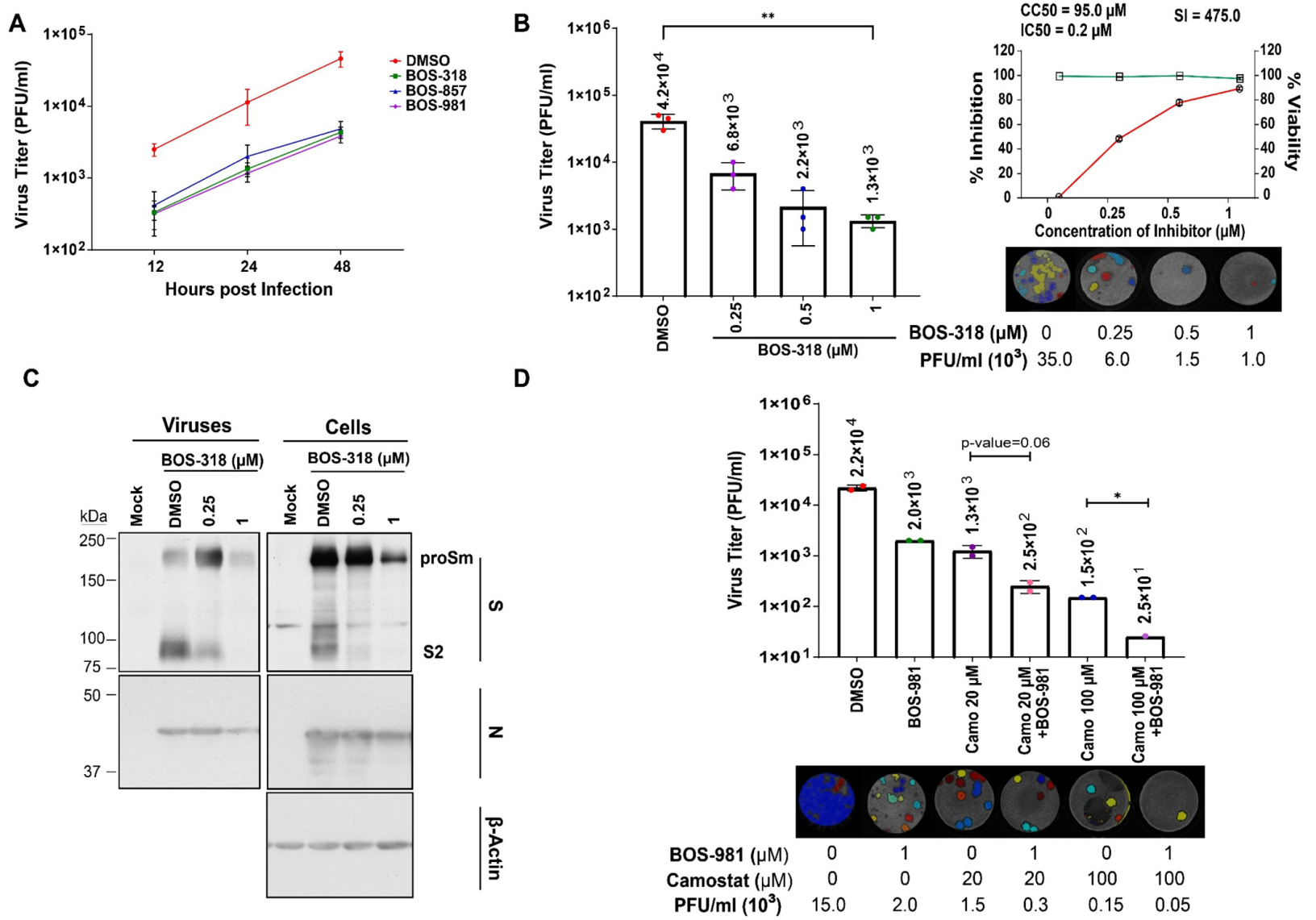

Role of furin & TMPRSS2 in SARS-CoV-2 infections and tropism

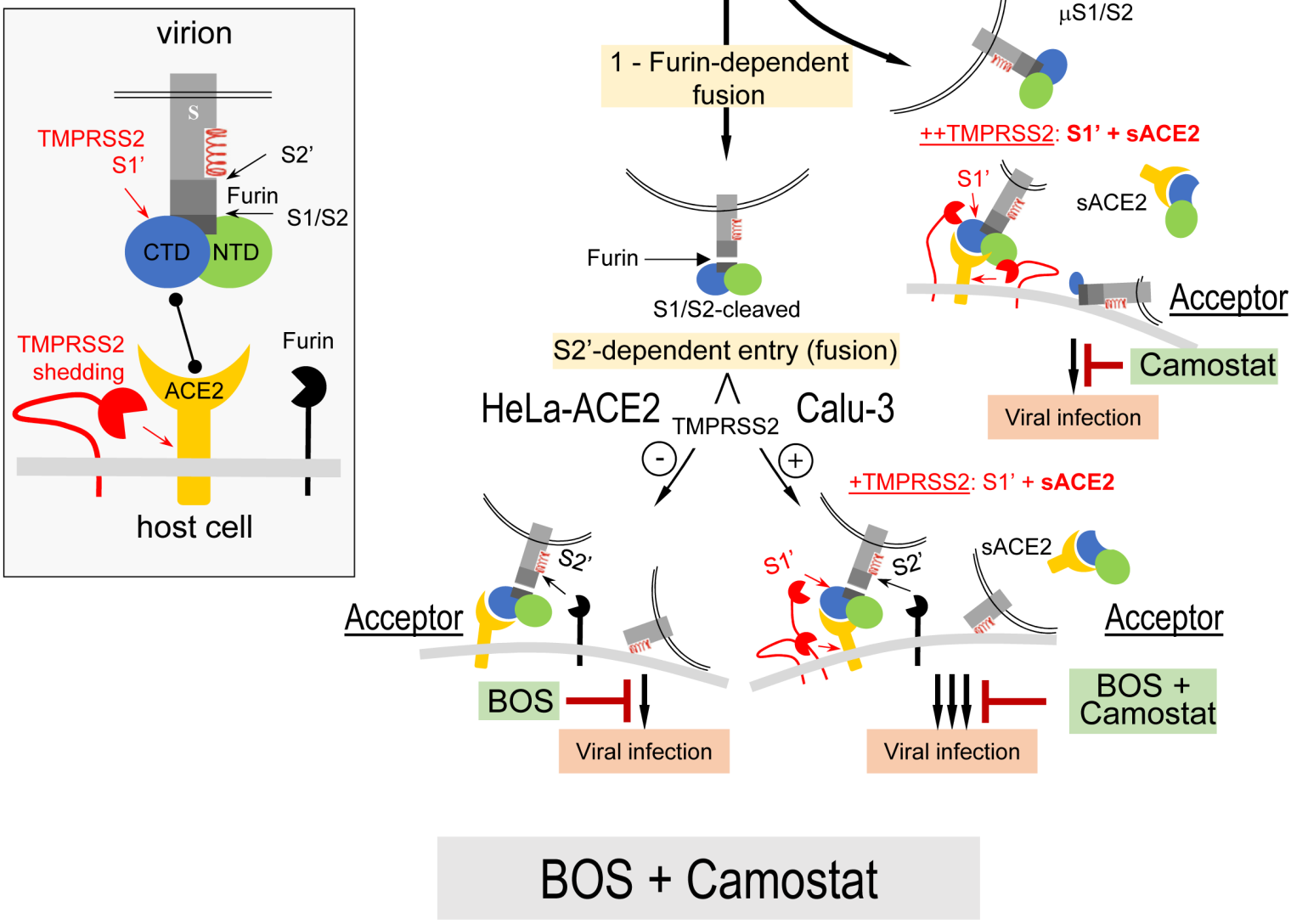

BOS + Camostat